A Unique Approach to Development of Near-Infrared Fluorescent Sensors for in Vivo Imaging

Lin Yuan, Weiying Lin,* Sheng Zhao, Wensha Gao, Bin Chen, Longwei He, and Sasa Zhu

State Key Laboratory of Chemo/Biosensing and Chemometrics, College of Chemistry and Chemical Engineering, Hunan University, Changsha 410082, P. R. China

Ⓢ *Supporting Information*

ABSTRACT: Near-infrared (NIR) fluorescent sensors have emerged as promising molecular tools for imaging biomolecules in living systems. However, NIR fluorescent sensors are very challenging to be developed. Herein, we describe the discovery of a new class of NIR fluorescent dyes represented by **1a/1c/1e**, which are superior to the traditional 7-hydroxycoumarin and fluorescein with both absorption and emission in the NIR region while retaining an optically tunable hydroxyl group. Quantum chemical calculations with the B3LYP exchange functional employing 6-31G(d) basis sets provide insights into the optical property distinctions between **1a/1c/1e** and their alkoxy derivatives. The unique optical properties of the new type of fluorescent dyes can be exploited as a useful strategy for development of NIR fluorescent sensors. Employing this strategy, two different types of NIR fluorescent sensors, **NIR-H$_2$O$_2$** and **NIR-thiol**, for H$_2$O$_2$ and thiols, respectively, were constructed. These novel sensors respond to H$_2$O$_2$ or thiols with a large turn-on NIR fluorescence signal upon excitation in the NIR region. Furthermore, **NIR-H$_2$O$_2$** and **NIR-thiol** are capable of imaging endogenously produced H$_2$O$_2$ and thiols, respectively, not only in living cells but also in living mice, demonstrating the value of the new NIR fluorescent sensor design strategy. The new type of NIR dyes presented herein may open up new opportunities for the development of NIR fluorescent sensors based on the hydroxyl functionalized reactive sites for biological imaging applications in living animals.

INTRODUCTION

Fluorescence imaging is a very powerful technique for localization and dynamic monitoring of biomolecules in living systems.[1−3] The development of new fluorescent imaging sensors has facilitated the recent significant advances in cell biology and medical diagnostic imaging.[4−6] Near-infrared (NIR) light (650−900 nm) is advantageous to be employed in biological imaging due to minimum photodamage to biological samples, deep tissue penetration, and minimum interference from background autofluorescence by biomolecules in the living systems.[7−9] However, small-molecule NIR fluorescent sensors are very challenging to be constructed. Thus, innovative strategies for development of NIR fluorescent sensors are actively sought after.

The traditional 7-hydroxycoumarins and fluorescein dyes contain a characteristic hydroxyl group (Figure 1), which can be modified to regulate their optical properties. This feature of the optically tunable hydroxyl group renders 7-hydroxycoumarins and fluorescein extensively employed in biochemical assays, optical sensing, and molecular optical imaging.[10] However, the absorption and emission wavelengths of the classic 7-hydroxycoumarin and fluorescein dyes only locate in the UV to visible region. Thus, they are not amenable for living animal imaging, in which the absorption and emission in the NIR region are highly desirable.

In this study, we described the discovery of a new class of NIR fluorescent dyes represented by **1a**, **1c**, and **1e** (Figure 1).

Significantly, the new class of NIR fluorescent dyes is superior to the traditional 7-hydroxycoumarin and fluorescein with absorption and emission in the NIR region while retaining an optically tunable hydroxyl group. In other words, the new type of fluorescent dyes enjoys the advantages of integrating tunable optical properties with NIR absorption and emission. This unique feature can be exploited for development of NIR fluorescent sensors for living animal imaging applications. Based on the design strategy, two innovative NIR fluorescent sensors for H$_2$O$_2$ and thiols were constructed. We demonstrate the utility of the novel NIR sensors in living animal imaging, highlighting the value of the new NIR fluorescent sensor design strategy.

RESULTS AND DISCUSSION

Synthesis of Fluorescent Dyes 1a−g. Unexpectedly, treatment of chloro-substituted cyanine **2a** or **2b** with resorcin **3a** in the presence of a base, NaH or triethylamine, at 50 °C for 4 h in DMF did not furnish the straightforward nucleophilic substitution product, but instead 2,3-dihydro-1H-xanthene-6-ol **1a** or **1c** (Scheme 1), respectively, was obtained. Similarly, compound **1e**, the analogue of compound **1a** with a chlorine atom nearby the phenolic alcohol, was also synthesized by the same route. The structures of compounds **1a**, **1c**, and **1e** were
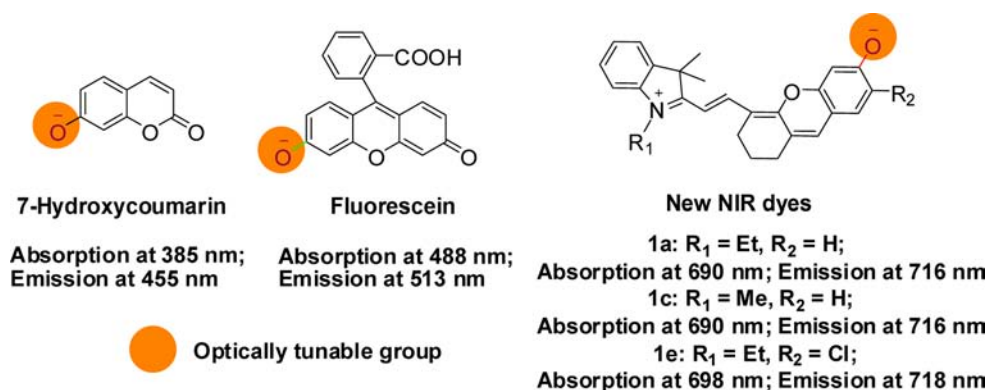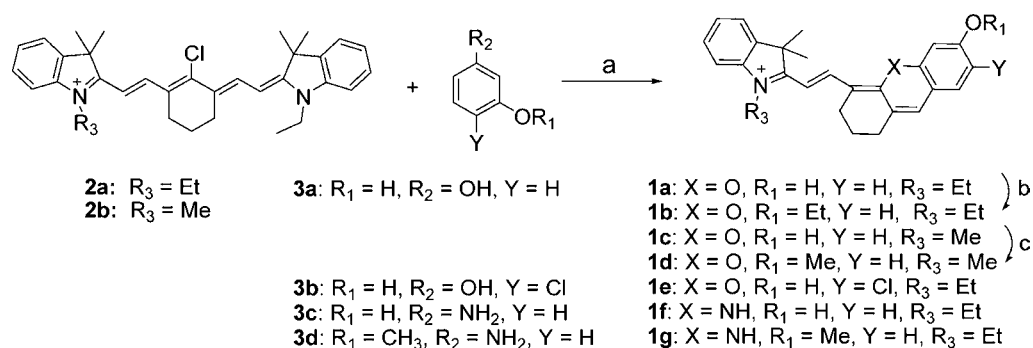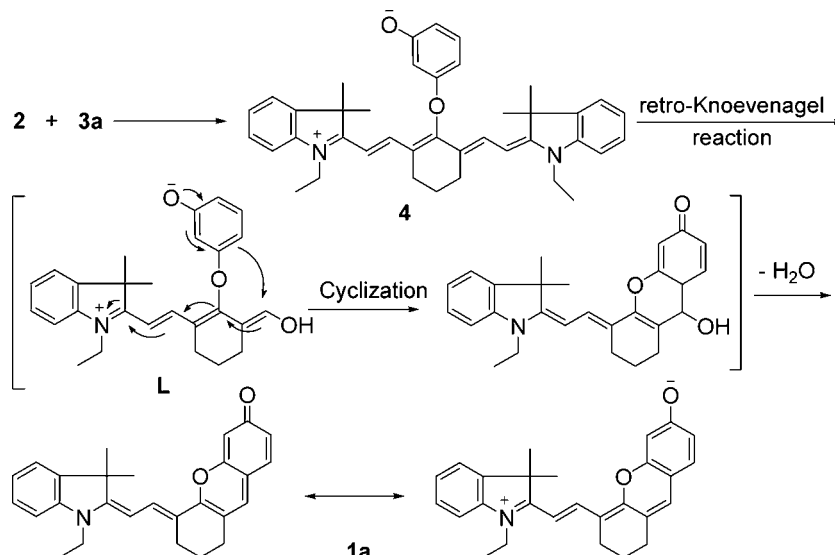
Figure 1. The chemical structures of the classic and new dyes bear an optically tunable hydroxyl group. The chemical structures and absorption/emission wavelengths of the classic dyes, such as 7-hydroxycoumarin and fluorescein, and the new NIR dyes reported herein (represented by **1a**, **1c**, and **1e**) with an optically tunable hydroxyl group.

Scheme 1. Structures and Synthesis of Compounds 1a–g[a]

[a]Conditions: (a) alkali, H_2O, and/or heating; (b) CH_3CH_2I, Cs_2CO_3; and (c) CH_3I, Cs_2CO_3.
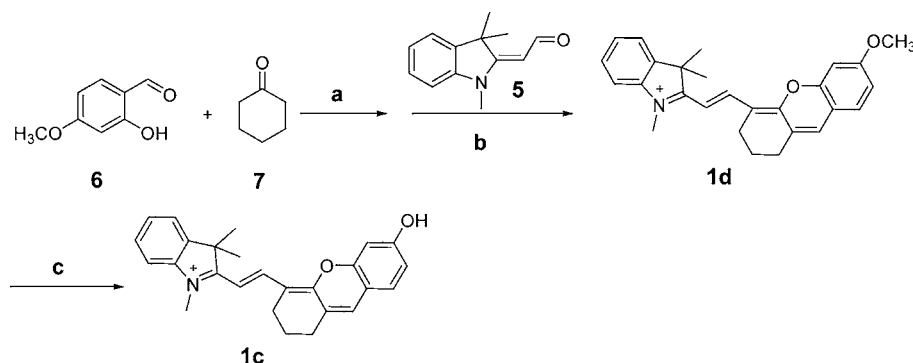
Scheme 2. A Proposed Reaction Mechanism for the Unique Formation of 2,3-Dihydro-1H-xanthene-6-ol Dyes Represented by 1a

characterized by ^1H and ^{13}C NMR and HRMS (ESI). Representative 2D COSY NMR spectra of compound **1c** further confirms the structure (Figure S1 and its description).

To get insight into the likely mechanism of the formation of the new compounds exemplified by **1a**, a number of control experiments were performed: 1) Compound **2a** was reacted with resorcin **3a** under the basic conditions at a lower temperature (25 °C) for 2 h to afford compound **4** (Schemes 2 and S1), the product arising from the straightforward nucleophilic substitution of chlorine atom; 2) The product **4** was isolated in pure form and further heated at 50 °C for 2 h in the presence of a base, resulting in formation of product **1a** (Scheme S1). Thus, the results of these control experiments

Scheme 3. Synthesis of Compounds 1c and 1d[a]

[a]Using a rational synthetic route based on the retrosynthesis analysis (Scheme S5) to corroborate the structures of this new type of compounds. Conditions: (a) EtOH, AcOH, piperidine, reflux; (b) Ac_2O, 50 °C; (c) BBr_3, CH_2Cl_2, 0 °C.
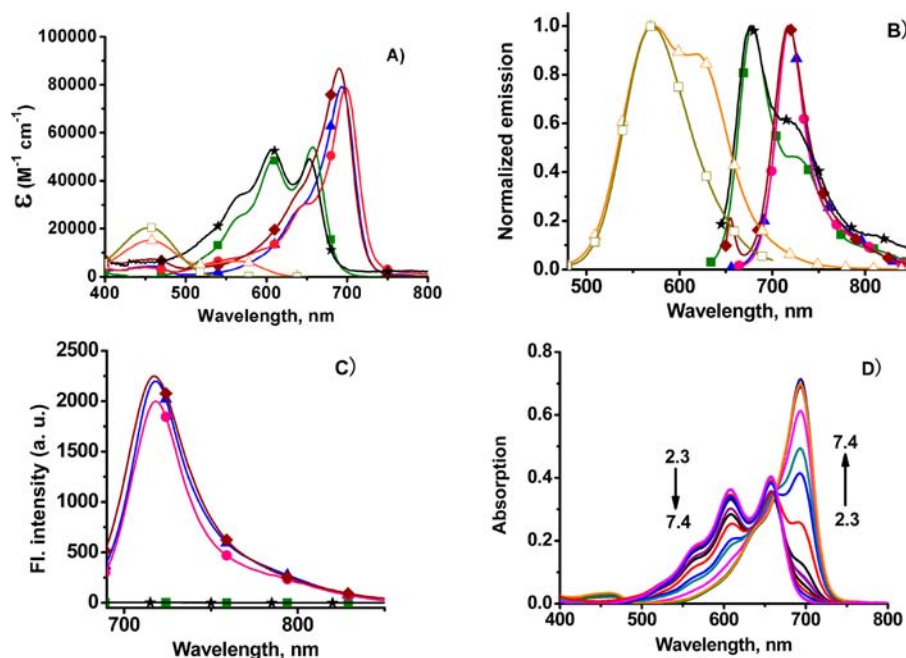

Figure 2. Absorption (A) and fluorescence emission spectra (B) of compounds **1a** (▲, blue), **1b** (■, green), **1c** (◆, purple), **1d** (★, black), **1e** (●, red), **1f** (△, orange, open), and **1g** (□, green, open) (10 μM) in pH 7.4 PBS/MeOH (1:1). (C) Fluorescence emission spectra of compounds **1a** (▲, blue), **1b** (■, green), **1c** (◆, purple), **1d** (★, black), and **1e** (●, red) (10 μM) in pH 7.4 PBS/MeOH (1:1). The emission spectra were obtained by excitation at the maximum absorption wavelength (B) or 690 nm (C), respectively. (D) pH-dependence of the absorption spectra of compound **1a** (10 μM) with the arrows indicating the change of the absorption intensities with pH enhancement from 2.3 to 7.4.

suggest that compound **4** is the possible intermediate in the mechanistic pathway.

Based on the above key findings, a plausible mechanistic pathway for the formation of 2,3-dihydro-1H-xanthene-6-ol dyes represented by **1a** is proposed in Scheme 2. We hypothesized that under stringent conditions, cyanine **4** could lose its Fischer's base by a retro-Knoevenagel reaction to give a putative half cyanine enol intermediate **L**. This hypothesis is based on the chemistry of cyanine dye formation that a half cyanine enol intermediate could condensate with Fischer's base to yield a cyanine dye,[11] and the Knoevenagel-type condensation reaction is reversible. The enol intermediate **L** could then undergo cyclization and dehydration reactions to furnish a much more stable product **1a**. Although the enol intermediate **L** was not isolated likely due to the facile subsequent steps of cyclization and dehydration, the similar chloro-substituted half cyanine enol could be furnished through

a retro-Knoevenagel reaction by heating cyanine **2a** at 50 °C under the basic conditions (Schemes S2 and S3). This further supports the proposed mechanism.

Additionally, the chloro-substituted half cyanine enol generated by heating cyanine **2a** at 50 °C under the basic conditions was isolated (Scheme S2). Then, the chloro-substituted half cyanine enol in pure form was further treated with resorcin **3a** in the presence of a base at 50 °C, which did not afford product **1a** (Scheme S4). Thus, this observation excludes the possibility that chloro-substituted half cyanine enol is the intermediate in the formation of product **1a**, in good agreement with the proposed mechanism as shown in Scheme 2. The conversion of compound **4** to the product **1a** upon further heating at a higher temperature (Scheme S1) is interesting, indicating the delicate nature of cyanine chemistry that the reaction conditions can dramatically affect the structures of final products. Importantly, the formation of 2,3-

dihydro-1H-xanthene-6-ols **1a**, **1c**, and **1e** from cyanines **2a** and **2b** provides a unique pathway for the preparation of a wide variety of 2,3-dihydro-1H-xanthene-6-ol derivatives from the classic cyanines. It is worthy to note that this synthetic pathway, to our best knowledge, is unprecedented.

Compounds **1b** and **1d** (Scheme 1), the ethyloxy and methyloxy derivatives of compounds **1a** and **1c**, respectively, were synthesized as controls to investigate the role of the hydroxyl group on the modulation of absorption/emission profiles. Reaction of compound **1a** or **1c** with iodoethane or iodomethane, readily afforded compound **1b** or **1d**, respectively. In addition, we also prepared compounds **1f** and **1g** (Scheme 1), in which the hydroxyl/methoxy group is in the tetrahydroacridine ring. Compounds **1f** and **1g** could be used as references for compounds **1a**–**e** to examine the potential effect of different heteroatoms at the X-position on the optical properties.

To further corroborate the structures of this new type of compounds, we wondered whether they could also be independently prepared by a "rational" synthetic route based on a retrosynthesis analysis (Scheme S5). We envisioned that the intermediate oxonium **8** is unstable, thus these new dyes may be synthesized in one pot without isolation of the intermediate **8**. For a representative case, as shown in Scheme 3, reaction of commercially available hydroxylbenzaldehyde **6** and ketone **7** in EtOH with a few drops of AcOH and piperidine as the catalysts afforded a yellow residue, which was further treated with the commercially available Fisher aldehyde **5** in Ac$_2$O to give compound **1d**. Removal of the methyl group of **1d** by BBr$_3$ readily afforded compound **1c**. To verify that the compound **1c** synthesized from the different routes (unique route in Scheme 1 and rational route in Scheme 3) is the same compound, an equivalent mixture of them was taken via ^{1}H and ^{13}C NMR spectra. As shown in Figures S2 and 3, the mixture shows a single NMR spectrum. The same phenomenon is observed for compound **1d** (Figures S4 and 5). Furthermore, the mass, absorption, and emission spectra of compounds **1c** and **1d** synthesized from the different routes are essentially identical (Figures S6 and 7), further supporting that this class of new compounds can be obtained by different routes. Significantly, the observation that compounds **1c** and **1d** could be independently prepared by distinct synthetic routes (unique route in Scheme 1 and rational route in Scheme 3), further substantiating the structures of the new class of dyes.

Photophysical Properties of Fluorescent Dyes 1a–g. The absorption and emission profiles of compounds **1a**–**g** are shown in Figure 2, and the photophysical data are compiled in Table 1. Gratefully, compound **1a** displays both absorption and emission peaks in the NIR region with maximum at 690 and 716 nm, respectively, in pH 7.4 PBS/MeOH (1:1). Importantly, compound **1a** has a fluorescence quantum yield of 0.36, which is relatively large for a NIR dye. Furthermore, the Stokes shift of compound **1a** is 26 nm, comparable to typical cyanines. Thus, compound **1a** appears to be a promising NIR dye. On the other hand, the maximal absorption and emission peaks of the reference **1b** are at 656/606 and 677 nm, respectively, which are significantly blue-shifted when compared to those of compound **1a**. Furthermore, the fluorescence quantum yield of compound **1b** is only 0.007, much less than that of compound **1a**. This is attributed to the alkyloxy substituent of **1b** which reduces the electron-donating ability of the oxygen atom[1c] and thus forbids the formation of the zwitterionic resonance form. Thus, these data suggest that the

Table 1. Photophysical Data of the Dyes 1a–g in pH 7.4 PBS/MeOH (1:1)

	λ_{abs}/nm[a]	ε_{max} (10^4 M^{-1} cm^{-1})	λ_{em}/nm[b]	Φ_f[c]	pK_a[d]
1a	690	7.9	716	0.36	5.6
1b	656/608	5.4/4.9	677	0.007	–
1c	690	8.7	716	0.37	5.6
1d	654/608	4.9/5.3	677	0.006	–
1e	698	7.9	718	0.30	4.5
1f	454	1.5	565	0.009	5.1; 7.4
1g	454	2.0	565	0.006	5.1

[a]The maximal absorption of the dye. [b]The maximal emission of the dyes. [c]Φ_f is the relative fluorescence quantum yield estimated by using indocyanine green (ICG, $\Phi_f = 0.13$ in DMSO) for **1a**–**e** or rhodamine 6G ($\Phi_f = 0.95$ in water) for **1f**–**g** as a fluorescence standard.[14] [d]The pK_a was calculated according to the Henderson–Hasselbach-type mass action equation.[12]

optical properties of new NIR dye **1a** can be regulated by alkylation on the hydroxyl group. Like compounds **1a** and **1b**, the absorption and emission spectra of dyes **1c**–**d** exhibit the similar changes. Interestingly, compounds **1b**/**1d** exhibit a shoulder peak in the emission profiles, which may be attributed to the existence of distinct species in the ground state due to charge localization.[8l,m] Notably, compounds **1a**, **1c**, and **1e** display strong fluorescence when excited at 690 nm, while compounds **1b** and **1d** show almost no fluorescence when excited at 690 nm (Figure 2C). The large fluorescence difference (>200-fold) between these fluorophores (**1a**/**1e** vs **1b** or **1c** vs **1d**) implies a method to develop a new NIR fluorescence turn-on switch by breaking the C–O bond through a chemical reaction.

To further understand the role of the hydroxyl group playing on the photophysical properties, we investigated the pH effect on the absorption/emission profiles of compound **1a**. As shown in Figure 2D, with the enhancement of pH from 2.3 to 7.4, the absorption bands at around 656/608 nm, ascribed to the phenolic form of **1a**, undergo a red-shift to a peak at around 690 nm, attributed to the phenolate form of **1a** (Scheme S6). There is a well-defined isosbestic point at 662 nm in the absorption spectra, indicating the equilibrium of the phenolic and phenolate forms of **1a**. The pH-dependence of the emission profiles of compound **1a** is consistent with that of the absorption profiles. When excited at 690 or 645 nm, enhancement of pH from 2.3 to 7.4 leads to a fluorescence turn-on (Figure S8) or ratiometric (with a red-shift) response (Figure S9), respectively. The pK_a of compound **1a** was calculated to be 5.6 based on the Henderson–Hasselbach-type mass action equation.[12] Like compound **1a**, compounds **1c** and **1e** also exhibit the absorption and emission peaks in the NIR region (Figure 2 and Table 1) and show the similar pH-dependent absorption (Figures S10 and S12) and fluorescence (Figures S11 and S13) changes. However, the pK_a of compound **1e** was calculated to be 4.5, which is significantly lower when compared to that of compound **1a**. This indicates that the pK_a of 2,3-dihydro-1H-xanthene-6-ol-based NIR merocyanine dyes can be readily tailored by introducing electron-withdrawing groups nearby the phenolic alcohol.
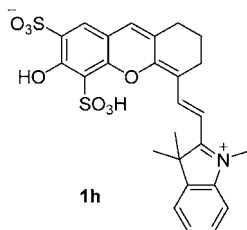
We also examined the absorption/emission properties of tetrahydroacridines **1f** and **1g** (Figure 2 and Table 1). However, compounds **1f** and **1g** show absorption and emission only in the visible region in pH 7.4 PBS/MeOH (1:1). This phenomenon may be ascribed to the pH-dependent equili-

brium between the neutral and the ionic forms of push—pull chromophores **1f** and **1g** (Scheme S7). In pH 7.4 PBS/MeOH (1:1), the neutral form is dominant. The neutral form may have relatively short absorption/emission wavelengths due to the weak push—pull system.[13] However, with the decrease of pH values, the ionic forms which have the strong push—pull system may become dominant, and a red-shift in absorption/emission is thus observed (Figures S14—15). Since tetrahydroacridines **1f** and **1g** only exhibit emission in the visible region at pH 7.4 and we were interested in the development of NIR dyes with potential for *in vivo* imaging applications, we decided to focus on 2,3-dihydro-1*H*-xanthene-6-ols **1a**, **1c**, and **1e** for further studies, as they have emission in the NIR region at pH 7.4.

Significantly, the above findings that there is a striking distinction between the optical properties of compounds **1a**/**1e** vs **1b** or **1c** vs **1d** indicate that the new class of NIR fluorescent dyes represented by **1a**, **1c**, and **1e** may be exploited as a novel strategy to design NIR fluorescent sensors by easy modifications on the hydroxyl group. By sharp contrast, regulation of the emission properties of the classic cyanines by photoinduced electron transfer (PET) is very challenging based on the Rehm—Weller equation.[9]

We further examined the photophysical properties of compounds **1a**, **1c**, and **1e** in biological media. Although compounds **1a**, **1c**, and **1e** appear to have limited solubility in water, they exhibit micromolar solubility in biological media. For example, compounds **1a**, **1c**, and **1e** have a solubility of approximately 6, 10, or 6 μM, respectively, in pure newborn calf serum (without addition of any co-organic solvent) estimated from the corresponding absorption spectra (Figure S16). In addition, these NIR dyes show strong fluorescence in pure newborn calf serum solution (Figure S17) with good fluorescence quantum yields over 0.2 (Table S1). The living cell fluorescence images and *in situ* (in cellulo) emission spectra of compounds **1a**, **1c**, and **1e** are shown in Figure S18. These results indicate that the new NIR dyes are cell permeable and have strong NIR fluorescence in living cells. Notably, the *in situ* (in cellulo) excitation and emission spectra of compounds **1a**, **1c**, and **1e** in HeLa cells resemble those of compounds **1a**, **1c**, and **1e** in pH 7.4 PBS/THF (1:1) (Figures S19—21), suggesting that the NIR emission of compounds **1a**, **1c**, and **1e** in living cells can be attributed to the single molecule of dyes. To demonstrate the feasibility of developing water-soluble NIR dyes, we have further synthesized compound **1h**, which bears several water-soluble groups (Schemes 4 and S8). As

Scheme 4. Structure of the Water-Soluble NIR Dye 1h

expected, dye **1h** is soluble in pure PBS and newborn calf serum (without addition of any co-organic solvent) with a solubility of at least 2 mM in PBS and 3 mM in newborn calf serum. The spectral properties of **1h** in pure PBS and newborn calf serum (Figures S22—23 and Table S1) resemble those of **1a**.

Theoretical Calculations. To get insight into the optical properties of the new functional dyes **1a**—**g**, density functional theory (DFT) calculations with the B3LYP exchange functional employing 6-31G(d) basis sets using a suite of Gaussian 09 programs were performed. Figures 3 and S24—28 show the representative optimized structures and molecular orbital plots (LUMO and HOMO) of the dyes **1a**—**g**. The C—C (N or O) bond lengths (in pm) of **1a**—**g** determined by DFT calculations are depicted in Tables S2—11. In the case of **1a** (phenolate form), the indolium moiety is essentially coplanar and conjugated with the 2,3-dihydro-1*H*-xanthene core (Figure 3). It is worthy to note that all the C—C bond lengths of the conjugated 2,3-dihydro-1*H*-xanthene-indolium backbone are very similar, at around 140 pm (Table S2). This value is the intermediate between the typical carbon—carbon single (154 pm) and the double (134 pm) bonds, attributed to the strong electronic delocalization and the partial decrease in the carbon—carbon bond length alternation (BLA, difference between consecutive single and double bonds) along the π-conjugated system.[13] This is further corroborated by the studies of the terminal C—N and C—O bond lengths in the conjugated system. The bond length of C14—N15 is 138 pm, which is the intermediate between the lengths of C—N bond (single bond, around 147 pm) and the iminium C=N (double bond, around 128 pm). The bond length of C1—O17 is 127 pm, which is relatively closer to C=O (double bond, around 121 pm) than C—O (single bond, around 144 pm), indicating that the O17 atom contributes pronouncedly to the π-conjugated system of the dye **1a** (phenolate form). The π electrons on the HOMO of **1a** (phenolate form) are mainly located on the whole π-conjugated 2,3-dihydro-1*H*-xanthene-indolium framework (including the O17 atom), but the LUMO is mostly positioned at the center of the conjugated 2,3-dihydro-1*H*-xanthene-vinyl bridge including the N15 atom (Figure 3), where the BLA is minimal. This distribution pattern of the π electrons on the HOMO/LUMO is a typical feature of cyanine dyes. Cyanines in the "cyanine limit" state feature a relatively sharp and intense absorption band in the NIR spectral range in light of the reduced vibronic contribution in the nonalternating (minimal BLA) structure.[13] Thus, the DFT calculation results are consistent with the absorption spectrum of **1a** (Figure 2A). The C1—O17 bond length of the compound **1b** is 135.3 pm (Table S3), which is longer than that (126.8 pm) of C1—O17 of the compound **1a** (phenolate form). This weakens the p—π conjugation between the O17 atom and the π-conjugated xanthene—indolium framework, and the energy levels of both HOMO and LUMO of the compound **1b** decrease relative to those of the compound **1a** (Figure 3). Upon close examination reveals that the π electrons on the HOMO and LUMO of **1b** are primarily located on the π-conjugated xanthene—indolium framework and the conjugated 2,3-dihydro-1*H*-xanthene-vinyl bridge, respectively. When compared to compound **1a**, the O17 atom of compound **1b** contributes less to the HOMO/LUMO. This suggests that the alkylation on the O17 atom indeed decreases the electron-donating ability of the oxygen atom, and compound **1b** loses its "cyanine limit" structure to some extent. In other words, the alkylation on O17 atom hinders the resonance between the O17 atom and the xanthene—indolium core. In addition, time-dependent DFT (TDDFT) calculations indicate that the excitation HOMO—LUMO energy gap between the S_0 state and the S_1 excited state of **1b** (2.27 or 2.09 eV based on the optimized S_0 or S_1 state geometry) is markedly higher than that of **1a** (phenolate form) (2.13 or 2.02

13514

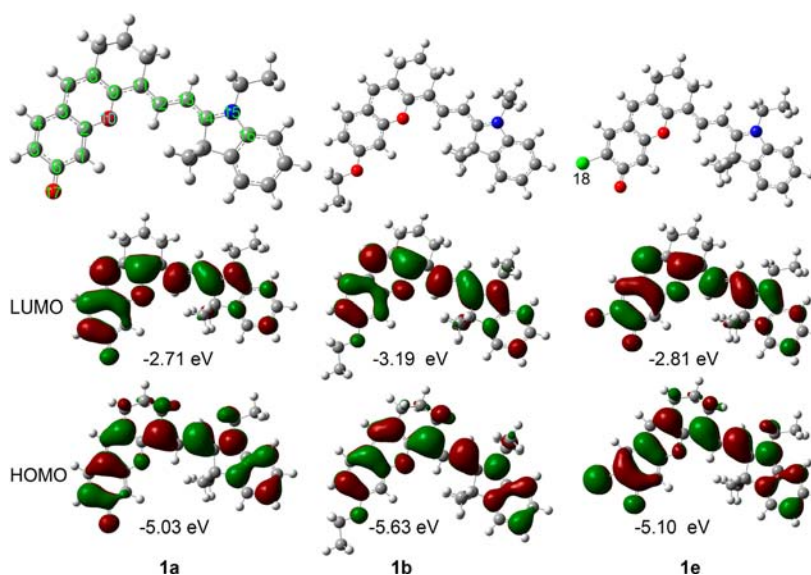dx.doi.org/10.1021/ja305802v | *J. Am. Chem. Soc.* 2012, 134, 13510—13523

Figure 3. DFT optimized structures and molecular orbital plots (LUMO and HOMO) of dyes **1a** (phenolate form), **1b**, and **1e** (phenolate form) in MeOH based on the optimized ground-state geometry (S$_0$). In the ball-and-stick representation, carbon, nitrogen, and oxygen atoms are colored in gray, blue, and red, respectively.

eV based on the optimized S$_0$ or S$_1$ state geometry) (Figure S24), which is in good agreement with the observation that the measured absorption and emission wavelength of **1b** is shorter than that of **1a**. The pH-dependence of the absorption spectra of compound **1a** (Figure 2D) can be explained in a similar manner (Figure S25 and Tables S4). In addition, the drastic distinction between the optical properties of the dyes **1c** and **1d** also can be rationalized analogously (Figure S26 and Tables S5 and S6).

The dye **1e** is the analogue of **1a** with an electron-withdrawing chlorine (Cl18) nearby the O17 atom. However, the energy levels of HOMO/LUMO of **1e** (phenolate form) are relatively lower than those of **1a** (phenolate form) due to the electron-withdrawing effect of chlorine, which stabilizes the aromatic system by electron delocalization (Figure 3). This may explain the above observation that the dye **1e** has a lower pK_a value than dye **1a**. In addition, TDDFT calculations indicate that the presence of the electron-withdrawing chlorine on the aromatic system also decreases the excited-state energy (about 0.03 eV), which corresponds to a bathochromic shift of 7 nm in the absorption maximum of **1e** with respect to **1a** (Table 2). Interestingly, this red-shift between compounds **1e** and **1a** obtained based on the TDDFT calculations is in good agreement with the value (8 nm) acquired experimentally (Table 2).

Dyes **1f** and **1g**, the tetrahydroacridine derivatives, show the pH-dependent equilibrium between the neutral and the ionic forms of push−pull chromophores (Scheme S7). DFT calculation indicates that the C9−C11 bond (148 pm) in the neutral form of the dye **1f** is relatively closer to the carbon−carbon single bond (154 pm) than the carbon−carbon double bond (134 pm) (Figure S27, Table S8) and that the π electrons on the LUMO of **1f** (neutral form) are principally located on the whole π-conjugated tetrahydroacridine moieties, but the HOMO is mostly positioned at the indolium−vinyl bridge moieties. Thus, at pH 7.4, when compared to **1a** (phenolate form), **1f** (neutral form) loses the cyanine limit to some extent. By contrast, in the ionic form of the dye **1f**, all the C−C bond lengths of the conjugated tetrahydroacridine−indolium back-

Table 2. TDDFT Excitation Energies (and Corresponding Excitation/Absorption Wavelengths) and Experimental Absorption Wavelengths of the Dyes 1a−g in MeOH

		theory[a]		experiment
	form	ΔE, eV[b]	λ_{abs}, nm	λ_{abs}, nm
1a	phenolate	2.13	583	690
	phenolic	2.29	542	608
1b		2.27	547	606
1c	phenolate	2.13	583	690
	phenolic	2.29	543	608
1d		2.27	546	606
1e	phenolate	2.10	590	698
	phenolic	2.27	545	610
1f	neutral	2.59	479	454
	ionic form	2.33	533	578
1g	neutral	2.58	480	454
	ionic	2.32	535	582

[a]The calculations are determined using B3LYP/6-31G(d) exchange−correlation functionals and basis sets. [b]The excitation HOMO−LUMO energy gap.

bone are very similar, at around 140 pm (Figure S27 and Table S9), ascribed to the strong electronic delocalization and the partial decrease in the carbon−carbon BLA along the π-conjugated system.[13] Furthermore, the π electrons on the HOMO of **1f** (the ionic form) are mainly located on the whole π-conjugated tetrahydroacridine−indolium framework, but the LUMO is mostly positioned at the center of the conjugated tetrahydroacridine−vinyl bridge (Figure S27), where the BLA is minimal. In addition, TDDFT calculations indicate that the excitation HOMO−LUMO energy gap of **1f** (neutral form, 2.59 eV) is significantly higher than that of **1f** (ionic form, 2.33 ev) (Table 2), which is in good agreement with the observation that **1f** exhibits a red-shift at lower pH values (Figure S14). The pH-dependent absorption spectra of **1g** (Figure S15a) also can be explained in a similar manner (Figure S28 and Tables S10−11).
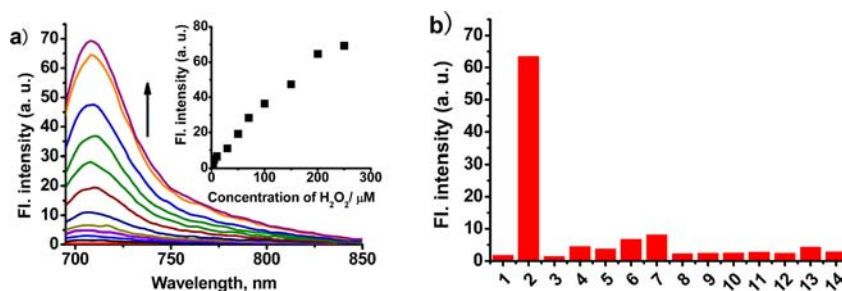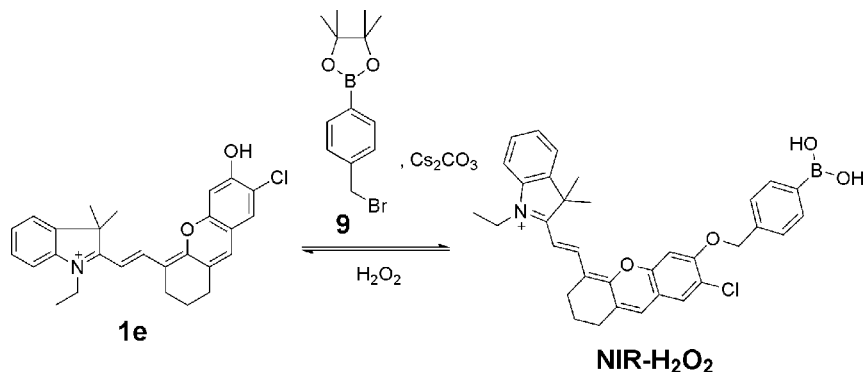
13515

dx.doi.org/10.1021/ja305802v | *J. Am. Chem. Soc.* 2012, 134, 13510−13523

Scheme 5. Design and Synthesis of NIR Fluorescent Turn-on H$_2$O$_2$ Sensor NIR-H$_2$O$_2$

Figure 4. (a) Fluorescence spectra of **NIR-H$_2$O$_2$** (1 μM) in the presence of various concentrations of H$_2$O$_2$ (0−250 μM) in phosphate buffer (pH 7.4, 1% DMSO) with excitation at 690 nm. Inset: Fluorescence intensity of **NIR-H$_2$O$_2$** (1 μM) at 708 nm vs H$_2$O$_2$ concentration (0−250 μM). (b) Fluorescence intensity (at 708 nm) of **NIR-H$_2$O$_2$** (1 μM) with excitation at 690 nm in the presence of various species (250 μM): 1, blank; 2, H$_2$O$_2$; 3, CH$_3$COOOH; 4, HOCl; 5, O$_2^-$·; 6, NO; 7, ·OH; 8, Fe^{3+}; 9, GSH; 10, NO$_2^-$; 11, NO$_3^-$; 12, TBHP; 13, vitamin C; 14, ·O^{t}Bu.

TDDFT calculations suggest that the maximal absorption bands of **1a−g** are attributed to the $S_1 \leftarrow S_0$ transition and that the maximal emission bands of **1a−b** are attributed to the $S_0 \leftarrow S_1$ transition. The calculated maximum of absorption or emission is shorter than that obtained experimentally (Table 2 and Figure S24), which is consistent with the previous report that TDDFT calculations may underestimate the excitation or emission wavelength due to the limitation of the exchange−correlation functional.[15] However, the deviations between the experimental values and TDDFT data are often systematic and can be corrected using appropriate linear scaling approaches. Indeed, for **1a−g**, as illustrated in Figure S29, the underestimated absorption maximum is rather systematic, and the linear regression is characterized by a correlation coefficient close to one. The experimental values and TDDFT data can be well correlated by the following expression:

$$\lambda_{\text{experiment}} = -618.532 + 2.245 \times \lambda_{\text{theory}} \quad (1)$$

Development of a New NIR Fluorescent Turn-on Sensor for H$_2$O$_2$ and the Applications for Biological Imaging in Living Mice. Reactive oxygen species (ROS) play important roles in many physiological and pathological processes.[16] Hydrogen peroxide (H$_2$O$_2$), one of the key ROS, is produced by activation of NADPH oxidase complexes during cellular stimulation with cytokines, neurotransmitters, and peptide growth.[16e−h] H$_2$O$_2$ serves as a signaling molecule in a wide variety of signaling transduction processes, an oxidative stress marker in aging and disease, and a defense agent in response to pathogen invasion.[16e−h,17] However, aberrant production of H$_2$O$_2$ is associated with various diseases including cancer, diabetes, neurodegenerative disorders, and cardiovascular.[18,19] Thus, it is of importance to monitor

generation and dynamic fluctuation of H$_2$O$_2$ in living systems. The construction of fluorescent sensors for H$_2$O$_2$ has attracted great attention.[20,21] However, the development of fluorescent H$_2$O$_2$ sensors with both maximal absorption and emission wavelengths in the NIR region (650−950 nm) is very challenging, although it is highly desirable for biological imaging of H$_2$O$_2$ in living animals.

Herein, employing the approach established above based on the optical property studies of the new type of NIR fluorescent dyes, we present **NIR-H$_2$O$_2$** (Scheme 5) as an innovative NIR fluorescent sensor for H$_2$O$_2$. The key features of **NIR-H$_2$O$_2$** include absorption and emission in the NIR region, a very large fluorescence turn-on response, high selectivity for H$_2$O$_2$, and suitability for imaging H$_2$O$_2$ in both living cells and living mice.

Figure 4a shows the changes in the fluorescence emission spectra when H$_2$O$_2$ was added in phosphate buffer containing the sensor **NIR-H$_2$O$_2$** (1 μM). The free sensor is almost nonfluorescent in the absence of H$_2$O$_2$ when excited at around 690 nm. However, upon addition of increasing concentrations of H$_2$O$_2$ (0−250 μM), a large fluorescence turn-on response (up to 180-fold enhancement at 708 nm) was observed (Figure 4a). Notably, this is a great enhancement factor for an NIR fluorescent sensor. The changes in the absorption spectra (Figure S30) are consistent with the variations in the emission profiles. Notably, the NIR sensor **NIR-H$_2$O$_2$** can respond to H$_2$O$_2$ in pure newborn calf serum (without addition of any co-organic solvent) (Figure S31).

Kinetics measurements of reaction of **NIR-H$_2$O$_2$** (1 μM) with H$_2$O$_2$ (100 μM) under the pseudo-first-order conditions give an observed rate constant of $k_{\text{obs}} = 2.95 \times 10^{-3}$ s^{-1}. As exhibited in Figure 4b, **NIR-H$_2$O$_2$** is highly selective to H$_2$O$_2$ over other typical ROS and biorelevant species, such as
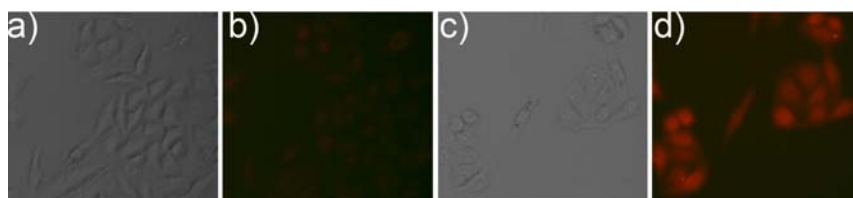
Figure 5. Images of HeLa cells treated with the sensor **NIR-H₂O₂**. (a) Brightfield image of HeLa cells incubated with only **NIR-H₂O₂** (1 μM) for 30 min; (b) fluorescence image of (a); (c) brightfield image of HeLa cells incubated with **NIR-H₂O₂** (1 μM) for 30 min and then further treated with H₂O₂ (10 μM); and (d) Fluorescence image of (c).
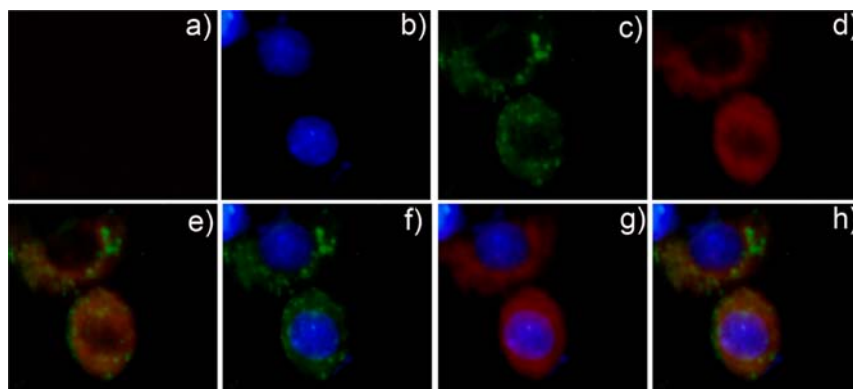

Figure 6. Imaging of H₂O₂ in living cells. (a) Fluorescence image of RAW 264.7 macrophages cells costained with **NIR-H₂O₂** for 60 min from red channel. (b−h) Fluorescence images of RAW 264.7 macrophages cells stimulated with PMA (3.0 μg/mL) and costained with **NIR-H₂O₂**, Hoechst 33258 (4.5 μM), and MitoTracker green for 60 min: (b) from blue channel (nuclear staining); (c) from green channel (mitochondria staining); (d) from red channel; (e) overlay of the green and red channels; (f) overlay of the blue and green channels; (g) overlay of the blue and red channels; and (h) overlay of the blue, green, and red channels.
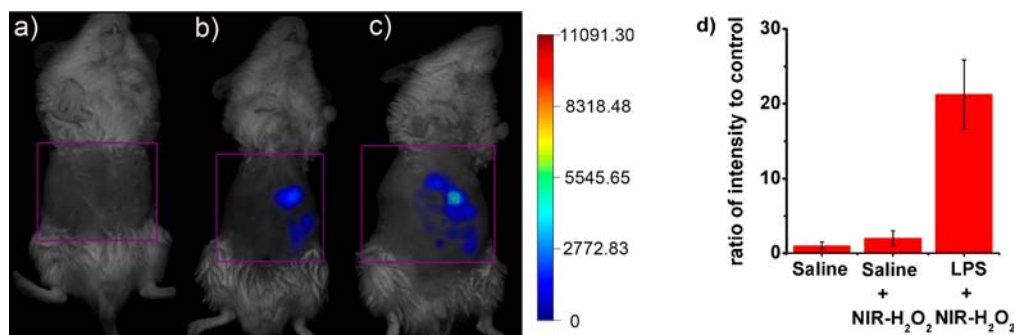

Figure 7. Representative fluorescent images (pseudo-color) of *in vivo* H₂O₂ production from the peritoneal cavity of the mice with **NIR-H₂O₂** during an LPS-mediated inflammatory response: (a) Neither LPS nor **NIR-H₂O₂** was injected for the negative control; (b) saline was injected in the ip cavity of mice, followed by ip injection of **NIR-H₂O₂** (160 nanomoles); and (c) LPS was injected into the peritoneal cavity of the mice, followed by ip injection of **NIR-H₂O₂** (160 nanomoles).The mice were imaged using a FMT 2500 LX quantitative tomography *in vivo* imaging system with an excitation filter of 670 nm and an emission range of 690−740 nm 30 min after the **NIR-H₂O₂** injection. (d) Quantification of fluorescence emission intensity from the abdominal area of the mice of groups a−c.
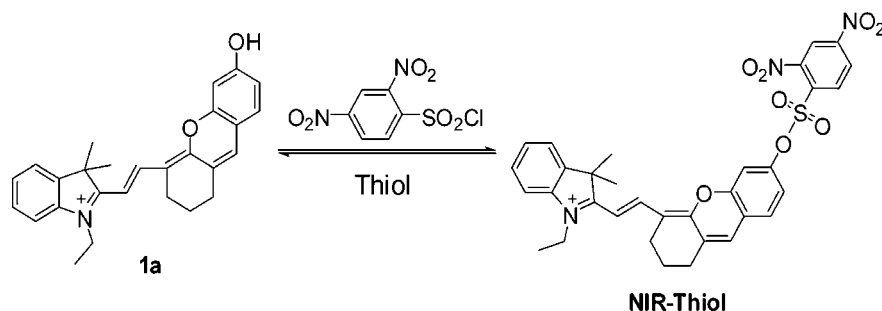
CH₃COOOH, HClO/⁻OCl, O₂⁻·, NO, ·OH, Fe³⁺, GSH, NO₂⁻, NO₃⁻, *tert*-butyl hedroperoxide (TBHP), vitamin C, and ·O^{t}Bu. The high selectivity and the sensing mechanism of the sensor **NIR-H₂O₂** to H₂O₂ may be attributed to the unique chemical properties of H₂O₂, as described previously by Chang's group.[20d]

We proceeded to evaluate the ability of the sensor **NIR-H₂O₂** to operate in live cells. HeLa cells incubated with **NIR-H₂O₂** (5 μM) for 30 min at 37 °C provide almost no fluorescence (Figure 5b). However, when the living HeLa cells loaded with **NIR-H₂O₂** were further treated with H₂O₂, they gave strong fluorescence (Figure 5d). These results imply that **NIR-H₂O₂** is cell membrane permeable and responsive to H₂O₂ in the living cells. In addition, the *in situ* (in cellulo)

emission spectrum of the sensor **NIR-H₂O₂** in the presence of H₂O₂ in HeLa cells resembles to that of compound **1e** in pH 7.4 PBS/THF (1:1) (Figure S32), suggesting that the NIR emission of the sensor **NIR-H₂O₂** in living cells can be attributed to the single molecule state.

Encouraged by the above promising results, we decided to further examine the feasibility of the sensor **NIR-H₂O₂** to detect endogenously produced H₂O₂ in living macrophage cells. When stimulated by phorbol myristate acetate (PMA), macrophage cells may produce endogenous H₂O₂.[22] The living RAW264.7 macrophage cells loaded with only the NIR sensor **NIR-H₂O₂** (1 μM) display almost no fluorescence (Figure 6a). However, the macrophage cells coincubated with PMA (3.0 μg/mL) and the sensor **NIR-H₂O₂** (1 μM) exhibit a dramatic

Scheme 6. Design and Synthesis of NIR Fluorescent Turn-on Thiol Sensor NIR-Thiol

enhancement in the red emission (Figure 6d). These data indicate that the new NIR sensor **NIR-H₂O₂** is capable of fluorescent imaging of endogenously produced H_2O_2 in the living RAW264.7 macrophage cells. Notably, the MTT assays (Figure S33)[28] indicate that **NIR-H₂O₂** of concentrations below 60 μM have no marked cytotoxicity. In addition, the mitochondria staining experiments (Figure 6c,e,h, and Figure S34) suggest that the sensor mainly associates with the mitochondria of RAW264.7 macrophage cells.

The major advantage of the new **NIR-H₂O₂** over the sensors based on traditional 7-hydroxycoumarin and fluorescein is that our **NIR-H₂O₂** has both absorption and emission in the NIR region. Thus, the unique NIR properties of **NIR-H₂O₂** render **NIR-H₂O₂** highly favorable for fluorsecence imaging of endogenously produced H_2O_2 in living animals. To examine this possibility, the sensor was treated with living mice. The H_2O_2 production *in vivo* was generated by activated macrophages and neutrophils in a lipopolysaccharide (LPS) model of acute inflammation.[23] The ICR mice were divided into three groups: Group one was untreated as the control group; the second group was given saline (400 μL) in the peritoneal cavity, followed by intraperitoneal (ip) injection with the sensor **NIR-H₂O₂** (160 nanomoles); and the third group was given an ip injection of LPS (1 mg in 400 μL saline) and followed by ip injection with the sensor **NIR-H₂O₂** (160 nanomoles) after 4 h. The mice were anaesthetized, and the abdominal fur was removed. The mice were imaged using a FMT 2500 LX quantitative tomography *in vivo* imaging system 30 min after the sensor injection. The mice treated with both LPS and the sensor exhibit a significantly higher fluorescence readout (pseudo-color) (Figure 7c) than the mice untreated (Figure 7a) or treated with only the sensor (Figure 7b). The fluorescent intensity from the abdominal area of the mice was quantified, and the data indicate that the mice loaded with LPS and the sensor have approximately 10- and 20-fold higher fluorescence intensity than the mice loaded with saline and the sensor and the mice loaded with saline, respectively (Figure 7d). Thereby, these results demonstrate that the new NIR sensor **NIR-H₂O₂** is suitable for imaging endogenously produced H_2O_2 in the living animals.

Development of a Novel NIR Fluorescent Turn-on Sensor for Thiols and the Applications for Biological Imaging in Living Mice. To further test the robust nature of the approach for NIR sensor development, we constructed **NIR-thiol** (Scheme 6) as a novel NIR fluorescent thiol sensor. Small molecular weight biological thiols play a critical role in many biological processes. However, abnormal levels of thiols are implicated in a variety of diseases including liver damage, skin lesions, and slowed growth.[24,25] Thus, it is of high interest to monitor biological thiols. A number of fluorescent thiol

sensors have been developed.[26] However, the applications of them have been largely limited to cell culture, thin specimens, and blood specimens, owing to the need for ultraviolet or visible light excitation. Thus, the development of NIR fluorescent thiol sensors with both absorption and emission in the NIR for imaging of thiols in living mice remains a major challenge in the field of optical imaging. Toward this end, we prepared compound **NIR-thiol** as a novel candidate of NIR fluorescent thiol sensor by modifications on the hydroxyl group of NIR dye **1a** with 2,4-dinitrobenzenesulfonate moiety[27] (Scheme 6) for optical imaging of endogenous thiols in living mice for the first time.

As designed, the free sensor **NIR-thiol** is essentially nonfluorescent in PBS buffer (Figure 8). However, the addition
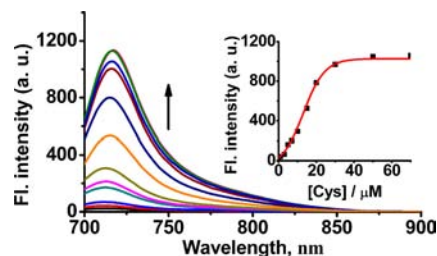

Figure 8. Fluorescence spectra of **NIR-thiol** (10 μM) in the presence of various concentrations of Cys (0−70 μM) in pH 7.4 PBS/CH₃CN (7:3) with excitation at 690 nm. Inset: Fluorescence intensity of **NIR-thiol** (10 μM) at 716 nm vs Cys concentration (0−70 μM).

of representative thiol, cysteine (Cys), elicited a dramatic change in the fluorescence spectra. A strong new emission peak at 716 nm appeared with a 50-fold enhancement. As displayed in the inset of Figure 8, low-micromolar thiols can be readily detected. Thus, the sensor should be sensitive enough to monitor intracellular thiols, which typically are in the millimolar level. The changes in the absorption spectra (Figure S35) are consistent with the variations in the emission profiles. The time course of the fluorescence intensity at 716 nm in the absence or presence of Cys was exhibited in Figure S36. Upon introduction of Cys, a significant enhancement in the emission intensity was noted, and the intensity essentially reached maximum within 60 s. This indicates that **NIR-thiol** responds very rapidly to thiols, and the sensor may have potential for monitoring of thiols in real time. Notably, the free sensor **NIR-thiol** is stable in the assay conditions over 24 h (Figure S36B), and the free sensor in the solid form can be stored for more than one year. As shown in Figure S37, **NIR-thiol** is highly selective to typical small molecular weight biological thiols (Cys, Hcy, and GSH) over other biorelevant species, such as Phe, Gly, Arg, Lys, Tyr, Leu, glucose, Ser, and Val, suggesting
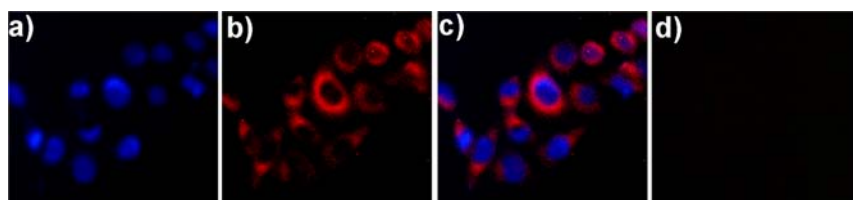
Figure 9. (a−c) Live Bel 7702 cells co-incubated with **NIR-thiol** (5 μM) and Hoechst 33258 (4.5 μM) for 30 min. (a) Emission from the blue channel (nuclear staining); (b) emission from the red channel; and (c) overlay of the blue and red channels. (d) Fluorescence image (red channel) of Bel 7702 cells pretreated with *N*-ethylmaleimide (1 mM) for 30 min and then incubated with **NIR-thiol** (5 μM) for 30 min.
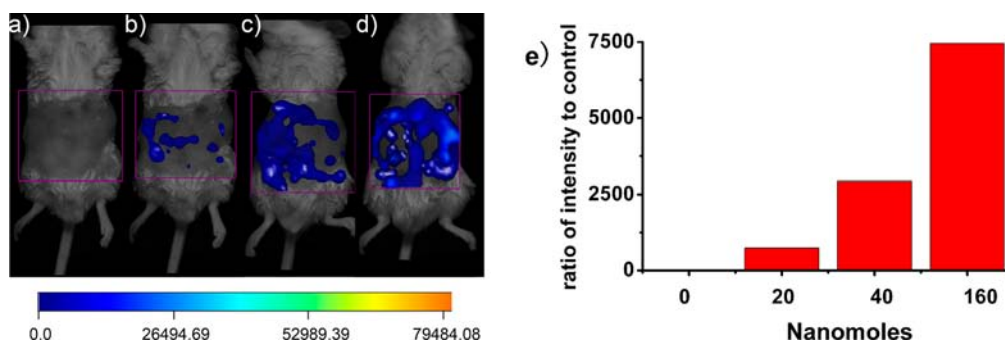

Figure 10. Representative fluorescence images (pseudo-color) for the mice ip injected with a different amount [(a) 0, (b) 20, (c) 40, or (d) 160 nanomoles] of **NIR-thiol**. (e) Quantification of the fluorescence intensities from the mice (ip) injected with a different amount (0, 20, 40, or 160 nanomoles) of **NIR-thiol**. The images were obtained 10 min after the injection of **NIR-thiol** into the ip cavity of the mice. The mice were imaged using a FMT 2500 LX quantitative tomography in vivo imaging system, with an excitation filter of 670 nm and an emission filter of 690−740 nm.

that the sensor is promising for applications in living systems. Furthermore, **NIR-thiol** can respond to thiols in pure newborn calf serum solution (without addition of any co-organic solvent) (Figure S38). The sensing mechanism of the sensor **NIR-thiol** can be attributed to the cleavage of the dinitrophenyl moiety by thiols.[27]

To assess the ability of the sensor **NIR-thiol** for NIR imaging of thiols in living cells, the sensor was incubated with living HeLa or Bel 7702 cells, and bright fluorescence was observed (Figures 9b, S39B). By contrast, in a control experiment, the HeLa or Bel 7702 cells were pretreated with *N*-ethylmaleimide (a thiol-reactive agent) and further incubated with **NIR-thiol**, where almost no fluorescence was noted (Figures 9d, S39D), suggesting the selective reaction of the sensor with thiols. Thus, the sensor appears to be cell membrane permeable and capable of NIR imaging of thiols in living cell. The NIR bioimaging is advantageous over visible bioimaging in terms of negligible background fluorescence of native cellular species. The *in situ* (in cellulo) emission spectrum of the sensor **NIR-thiol** in HeLa cells is very similar to that of compound **1a** in pH 7.4 PBS/THF (1:1) (Figure S40), suggesting that the NIR emission of **NIR-thiol** in living cells can be attributed to the single molecule state. In addition, the MTT assays (Figure S41)[28] indicate that **NIR-thiol** of concentrations below 50 μM does not show noticeable cytotoxicity.
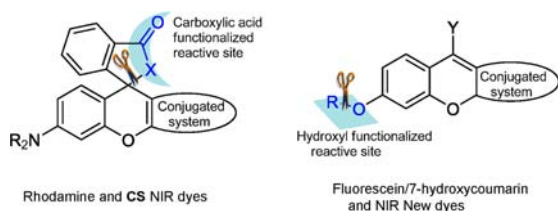
Thus, the prominent features of **NIR-thiol** include NIR absorption and emission, rapid response, high sensitivity, excellent selectivity, good cell membrane permeability, and low cytotoxicity. These desirable attributes prompted us to further examine the suitability of the sensor for visualizing endogenous thiols in living animals. A different amount (0, 20, 40, or 160 nanomoles) of **NIR-thiol** was injected into the ip cavity of mice. The mice were imaged using a FMT 2500 LX quantitative tomography *in vivo* imaging system 10 min after the **NIR-thiol** injection. As shown in Figure 10b, strong

fluorescence (pseudo-color) was noted for the mice injected with 20 nanomoles of **NIR-thiol**, whereas almost no fluorescence was observed in the control mice without being injected with the sensor (Figure 10a). In addition, the mice injected with a higher amount (40 or 160 nanomoles) of **NIR-thiol** provided brighter fluorescence (pseudo-color) (Figure 10c,d). Quantification of the fluorescence intensities from the mice (ip) injected with a different amount (0, 20, 40, or 160 nanomoles) of **NIR-thiol** reveals a dose-dependent increase in signal as a function of the sensor amount (Figure 10e). A very large signal-to-noise contrast ratio (*ca.* 700-fold enhancement) was observed for the mice injected with 20 nanomoles of **NIR-thiol**. In addition, the signal-to-noise contrast ratio jumped to *ca.* 2900- or 7400-fold enhancement when the mice were injected with 40 or 160 nanomoles of **NIR-thiol**, respectively. Taken together, these data indicate that **NIR-thiol** is a robust imaging agent for visualizing endogenous thiols in the context of living mice for the first time.

Previously, we have developed a class of NIR dyes, Changsha (**CS**) NIR dyes, which are superior to the traditional rhodamine dyes with both absorption and emission in the NIR region while retaining the rhodamine-like fluorescence on−off switching mechanism.[8n] Notably, there are drastic distinctions between the **CS** NIR dyes and the novel type of NIR dyes reported herein. First, the design strategies for these two types of dyes are largely different. The **CS** NIR dyes were rationally designed based on the "integration" of a benzoic acid moiety with a merocyanine unit inspired by the fact that the electronic pulling pathway for the **CS** NIR functional dye spirocyclization highly resembles that of the traditional rhodamine dye spirocyclization. By sharp contrast, the new type of NIR dyes described herein was constructed based on the new reaction between chloro-substituted cyanine with resorcin under basic conditions. In addition, the mechanistic studies reveal that the new reaction likely involves a cascade sequence of putative

retro-Knoevenagel, cyclization, and dehydration. Second, the **CS** NIR dyes may be "considered" as the NIR surrogates of the classic rhodamine dyes. By contrast, the new type of NIR dyes described herein appear to be the NIR surrogates of the traditional fluorescein/7-hydroxycoumarin dyes. Thus, more importantly, the distinction between the **CS** NIR and the new NIR dyes is in their use as platforms for fluorescent sensor design. Just like the rhodamine platform,[5j−1] the **CS** NIR dyes are mainly applicable for the design of fluorescent sensors based on the carboxylic acid functionalized reactive sites (Scheme 7).

Scheme 7. Schematic Illustration of the New NIR and CS NIR dyes, Fluorescein/7-Hydroxycoumarin, And Rhodamine As the Platforms for Fluorescent Sensor Design[a]

[a]Notably, the relationship between the new NIR and **CS** NIR dyes is just like that between fluorescein/7-hydroxycoumarin and rhodamine. They are essentially complementary but not replaceable.

Whereas, just like the fluorescein/7-hydroxycoumarin platform,[5l,10,20d] the new NIR dyes are primarily applicable for the design of fluorescent sensors based on the hydroxyl functionalized reactive sites (Scheme 7). For instance, the **CS** NIR dyes could be employed to design a NIR fluorescent sensor for HOCl based on thiosemicarbazide chemistry (a carboxylic acid functionalized reactive site),[8n] but they are not suitable for development of NIR fluorescent sensors for H_2O_2 and thiols based on the borate chemistry[20d] and 2,4-dinitrobenzenesulfonate chemistry[27] (hydroxyl functionalized reactive sites). On the other hand, the new NIR dyes could be used to construct NIR fluorescent sensors for H_2O_2 and thiols based on borate chemistry[20d] and 2,4-dinitrobenzenesulfonate chemistry[27] (hydroxyl functionalized reactive sites) as described in this work, but they are not applicable for development of an NIR fluorescent sensor for HOCl based on thiosemicarbazide chemistry (a carboxylic acid functionalized reactive site).[8n] In other words, from the fluorescent sensor design point of view, the novel type of NIR and the **CS** NIR dyes have different scopes and limitations. They are essentially complementary but not replaceable, just like the relationship between fluorescein/ 7-hydroxycoumarin and rhodamine.

CONCLUSION

Fluorescence microscopy with synthetic sensors offers a powerful technique for studying biomolecules in their native environment. NIR fluorescent sensors are advantageous over visible light fluorescent sensors as NIR light leads to minimum photodamage to biological samples, deeper tissue penetration, and minimum interference from background autofluorescence. Thus, robust strategies for design of NIR fluorescent sensors are highly sought after. In this study, we have successfully developed a new approach for ready construction of NIR fluorescent sensors based on a novel class of NIR dyes represented by **1a**, **1c**, and **1e**, which are superior to the traditional 7-hydroxycoumarin and fluorescein while retaining an optically tunable hydroxyl group. In addition, we have

performed quantum chemical calculations with the B3LYP exchange functional employing 6-31G(d) basis sets to shed light on the structure-optical properties of the new class of NIR dyes. Moreover, we have demonstrated that the approach can be easily employed to develop different types of NIR fluorescent sensors for biological imaging applications in the living animals: **NIR-H_2O_2** for endogenously produced H_2O_2 and **NIR-thiol** for endogenous thiols, highlighting the value of the new NIR fluorescent sensor design approach. We expect that the new NIR dyes described herein will serve as useful fluorescent platforms for the development of fluorescent sensors based on the hydroxyl functionalized reactive sites, a useful complement to our previously reported **CS** NIR dyes, which are mainly applicable for the design of fluorescent sensors based on the carboxylic acid functionalized reactive sites.

■ EXPERIMENTAL SECTION

Synthesis of Compound 1a. Resorcin **3a** (86.0 mg, 0.78 mmol) and NaH (60% in mineral oil, 19.1 mg, 0.78 mmol) or triethylamine (0.3 mL) were placed in a flask containing DMF (2 mL), and the mixture was stirred at room temperature under nitrogen atmosphere for 10 min. Compound **2a** (200.1 mg, 0.31 mmol) in DMF (1.0 mL) was introduced to the mixture via a syringe, and the reaction mixture was heated at 50 °C for 4 h. The solution was then removed under reduced pressure. The crude product was purified by silica gel flash chromatography using petroleum ether/CH_2Cl_2/MeOH (25: 25: 1) as eluent to give compound **1a** as a blue-green solid (90.4 mg, yield 55.0%). ^{1}H NMR (400 MHz, CDCl$_3$): δ 1.41−1.45 (t, J = 7.2 Hz, 3H), 1.69 (s, 6H), 1.88−1.91 (m, 2H), 2.63−2.66 (t, J = 5.6 Hz, 2H), 2.69−2.72 (t, J = 5.6 Hz, 2H), 4.07−4.12 (q, J = 6.8 Hz, 2H), 5.92− 5.96 (d, J = 14.0 Hz, 1H), 6.97−7.00 (2H), 7.06−7.08 (d, J = 8.0 Hz, 1H), 7.19−7.23 (t, J = 7.6 Hz, 1H), 7.24−7.26 (d, J = 8.8 Hz, 1H), 7.35−7.39 (3H), 8.37−8.40 (d, J = 14.0 Hz, 1H). ^{13}C NMR (100 MHz, CDCl$_3$): δ 12.09, 20.75, 24.35, 28.39, 39.29, 48.92, 97.80, 103.01, 107.87, 109.87, 114.85, 115.04, 121.25, 121.45, 122.29, 124.57, 128.63, 129.35, 139.01, 139.79, 140.58, 141.89, 156.87, 162.32, 170.76. HRMS (ESI) m/z calcd for $C_{27}H_{28}NO_2$ (M$^+$): 398.2115. Found: 398.2112.

Synthesis of Compound 1b. To a solution of compound **1a** (200.0 mg, 0.38 mmol) and iodoethane (592.8 mg, 3.80 mmol) in dry DMF (2.0 mL), Cs_2CO_3 (248.0 mg, 0.76 mmol) was added. The mixture was stirred at room temperature for 1 h, and then the solvent was evaporated under reduced pressure to give the crude product, which was purified by silica gel flash chromatography using petroleum ethyl acetate/acetone (3:1) as eluent to give compound **1b** as a blue solid (165.9 mg, 79.5%). ^{1}H NMR (400 MHz, CDCl$_3$): 1.40−1.48 (m, 6H), 1.74 (s, 6H), 1.87 (bs, 2H), 2.69 (bs, 4H), 4.11- 4.14 (q, J = 7.2 Hz, 2H), 4.40- 4.43 (q, J = 6.8 Hz, 2H), 6.30- 6.40 (dd, J = 14.8, 5.0 Hz, 1H), 6.76 (s, 1H), 6.77−6.84 (dd, 1H), 7.30−7.41 (m, 5H), 7.47− 7.49 (dd, J = 7.2, 2.0 Hz, 1H), 8.55−8.57 (d, J = 14.2 Hz, 1H). ^{13}C NMR (100 MHz, CDCl$_3$): δ 11.94, 13.65, 19.31, 23.67, 27.30, 28.16, 40.39, 49.56, 63.81, 100.21, 102.19, 111.42, 112.69, 113.92, 114.72, 121.69, 126.11, 126.21, 128.07, 128.26, 133.56, 140.02, 140.71, 144.59, 153.51, 161.09, 161.60, 175.38. HRMS (ESI) m/z calcd for $C_{29}H_{32}NO_2^+$ (M$^+$): 426.2428. Found: 426.2436.

Synthesis of Compound 1c. Route A (shown in Scheme 1): Resorcin **3a** (275.6 mg, 2.48 mmol) and triethylamine (0.3 mL) were placed in a flask containing DMF (2 mL), and the mixture was stirred at room temperature under nitrogen atmosphere for 10 min. Compound **2b** (400.0 mg, 0.83 mmol) in DMF (1.0 mL) was introduced to the mixture via a syringe, and the reaction mixture was heated at 50 °C for 5 h. The solution was then removed under reduced pressure. The crude product was purified by silica gel flash chromatography using petroleum ether/ethyl acetate (2:1) to CH_2Cl_2/ethanol (1:0 to 50:3) as eluent to give compound **1c** as a blue-green solid (252.4 mg, yield 59.5%).

Route B (shown in Scheme 3): Compound **1d** (200.2 mg, 0.44 mmol) was placed in a flask containing anhydrous CH$_2$Cl$_2$ (3 mL), and the solution was stirred at 0 °C under nitrogen atmosphere for 30 min. BBr$_3$ (1 mL BBr$_3$ dissolved in 3 mL CH$_2$Cl$_2$) was slowly introduced to the mixture via a syringe, and the reaction mixture was warmed to room temperature and stirred at room temperature for 24 h. The mixture was added to a saturated NaHCO$_3$ solution (50 mL) and was extracted with CH$_2$Cl$_2$ (50 mL) three times. The organic phases were combined and dried by anhydrous MgSO$_4$. The solution was then removed under reduced pressure. The crude product was purified by silica gel flash chromatography using petroleum ether/ethyl acetate (2:1) to CH$_2$Cl$_2$/ethanol (15:1) as eluent to give compound **1c** as a blue-green solid (182.6 mg, yield 89.7%).

^{1}H NMR (500 MHz, CDCl$_3$): δ 1.67 (s, 6H), 1.87−1.92 (m, 2H), 2.62 (t, J = 6.0 Hz, 2H), 2.67 (t, J = 6.0 Hz, 2H), 3.36 (s, 3H), 4.07−4.12 (q, J = 7.2 Hz, 2H), 5.60 (d, J = 13.5 Hz, 1H), 6.58 (s, 1H), 6.78 (dd, J = 9.0, 1.5 Hz, 1H), 6.84 (d, J = 8.0 Hz, 1H), 7.05 (t, J = 8.0 Hz, 1H), 7.21 (d, J = 9.0 Hz, 1H), 7.26−7.29 (2H), 7.32(s, 1H), 8.08 (d, J = 13.0 Hz, 1H). ^{13}C NMR (125 MHz, CDCl$_3$): δ 21.34, 24.52, 27.96, 28.59, 29.70, 30.08, 47.98, 94.47, 103.61, 107.82, 116.36, 116.51, 116.71, 122.02, 122.29, 127.37, 128.13, 129.79, 132.43, 139.59, 140.06, 143.87, 159.02, 159.91, 166.07. HRMS (ESI) m/z calcd for C$_{26}$H$_{26}$NO$_2^+$ (M$^+$): 384.1958. Found: 384.1971.

Synthesis of Compound 1d. Route A (shown in Scheme 1): To a solution of compound **1c** (200.0 mg, 0.39 mmol) and iodomethane (110.9 mg, 0.80 mmol) in dry DMF (2.0 mL), Cs$_2$CO$_3$ (248.0 mg, 0.76 mmol) was added. The mixture was stirred at room temperature for 1 h, and then the solvent was evaporated under reduced pressure to give the crude product, which was purified by silica gel flash chromatography using petroleum/ethyl acetate (1:1) to CH$_2$Cl$_2$/ethanol (15:1) as eluent to give compound **1d** as a blue solid (167.5 mg, 81.6%).

Route B (shown in Scheme 3): To a solution of 2-hydroxy-4-methoxybenzaldehyde **6** (1.0 g, 6.6 mmol) and cyclohexanone **7** (1.3 g, 13.2 mmol) in ethanol (50.0 mL) was added piperidine (0.6 mL) and acetic acid (0.2 mL). The mixture was heated and stirred at reflux condition for 12 h, and then the solvent was evaporated under reduced pressure to give a residue. The resulting residue was treated with Fisher aldehyde **5** (2.8 g, 14.0 mmol) in acetic anhydride (10 mL), and the mixture was heated and stirred at 50 °C for 8 h. Subsequently, the solvent was evaporated under reduced pressure to give the crude product which was further purified by silica gel flash chromatography using petroleum/ethyl acetate (3:1) to CH$_2$Cl$_2$/ethanol (1: 0 to 15:1) as eluent to afford compound **1d** as a blue solid (547.6 mg, 19.5%).

^{1}H NMR (400 MHz, CDCl$_3$): 1.82 (s, 6H), 1.91−1.97 (m, 2H) 2.74−2.77 (t, J = 6.0 Hz, 2H), 2.79−2.82 (t, J = 6.0 Hz, 2H), 3.98 (s, 3H), 4.04 (s, 3H), 6.49−6.53 (d, J = 14.8 Hz, 1H), 6.88−6.91 (2H), 7.29 (1H), 7.37−7.43 (3H), 7.46−7.51 (2H), 8.63−8.67 (d, J = 15.2 Hz, 1H). ^{13}C NMR (100 MHz, CDCl$_3$): δ 20.41, 24.85, 28.36, 29.32, 29.78, 34.50, 50.61, 56.60, 100.90, 104.36, 112.69, 113.49, 115.33, 115.89, 122.51, 127.32, 127.44, 128.99, 129.30, 134.19, 141.55, 142.27, 145.73, 154.62, 162.02, 163.24, 177.52; HRMS (ESI) m/z calcd for C$_{27}$H$_{28}$NO$_2^+$ (M$^+$): 398.2115. Found: 398.2127.

Synthesis of Compound 1e. 4-chloro resorcin **3b** (134.1 mg, 0.93 mmol) and triethylamine (0.3 mL) were placed in a flask containing DMF (2.0 mL), and the mixture was stirred at room temperature under nitrogen atmosphere for 10 min. Compound **2a** (200.0 mg, 0.31 mmol) in DMF (1.0 mL) was introduced to the mixture via a syringe, and the reaction mixture was heated at 75 °C for 4 h. The solution was then removed under reduced pressure. The crude product was purified by silica gel flash chromatography using CH$_2$Cl$_2$/EtOH (50:1) as eluent to give compound **1e** as a blue-green solid (60.7 mg, yield 35.0%). ^{1}H NMR (500 MHz, CDCl$_3$): δ 1.36−1.39 (t, J = 7.2 Hz, 3H), 1.67 (s, 6H), 1.89−1.92 (2H), 2.61−2.64 (t, J = 6.0 Hz, 2H), 2.68−2.70 (t, J = 6.0 Hz, 2H), 3.89−3.93 (q, J = 7.2 Hz, 2H), 5.67−5.70 (d, J = 13.5 Hz, 1H), 6.77 (s, 1H), 6.88−6.89 (d, J = 8.0 Hz, 1H), 7.08−7.11 (t, J = 7.5 Hz, 1H), 7.29−7.33 (3H), 7.41 (s, 1H), 8.13−8.16 (d, J = 13.5 Hz, 1H). ^{13}C NMR (125 MHz, CDCl$_3$): δ 11.66, 21.19, 24.44, 28.07, 28.57, 38.24, 47.90, 94.74, 103.82, 108.23, 115.22, 115.72, 117.54, 122.24, 122.87, 127.26, 128.27, 134.45, 139.19,

139. 97, 142.70, 157.42, 160.57, 166.39. HRMS (ESI) m/z calcd for C$_{27}$H$_{27}$NO$_2$Cl (M$^+$): 432.1725. Found: 432.1742.

Synthesis of Compound 1f. 3-aminophenol **3c** (338.0 mg, 3.11 mmol) and compound **2a** (197.8 mg, 0.31 mmol) were placed in a flask containing DMF (3.0 mL). After heating for 4 h at 80 °C under nitrogen, the solution was concentrated under reduced pressure. The resulting crude product was purified by silica gel flash chromatography using petroleum ether/CH$_2$Cl$_2$/MeOH (25:25:1) as eluent to give compound **1f** as a red solid (105.6 mg, yield 65.2%). ^{1}H NMR (400 MHz, CDCl$_3$): δ 8.33−8.36 (d, J = 12.8 Hz, 1H), 7.63 (s, 1H), 7.49−7.51 (d, J = 8.8 Hz, 1H), 7.41 (d, J = 2.4 Hz, 1H), 7.15−7.18 (m, 2H), 6.96−6.98 (dd, J = 8.8, 2.4 Hz, 1H), 6.84−6.88 (t, J = 7.2 Hz, 1H), 6.61−6.63 (d, J = 7.6 Hz, 1H), 5.54−5.58 (d, J = 12.8 Hz, 1H), 3.69−3.74 (q, J = 7.2 Hz, 2H), 2.87−2.90 (t, J = 6.0 Hz, 2H), 2.76−2.78 (t, J = 5.6 Hz, 2H), 1.91−1.97 (m, 2 H), 1.71 (s, 6H), 1.24−1.28 (t, J = 6.8 Hz, 3H). ^{13}C NMR (100 MHz, CDCl$_3$) 158.65, 157.89, 155.47, 147.82, 144.06, 139.59, 134.28, 128.44, 127.93, 127.51, 127.15, 124.07, 121.68, 121.43, 119.66, 117.79, 109.29, 105.88, 92.75, 46.00, 36.83, 30.48, 28.46, 26.51, 22.41, 10.99; HRMS (EI) m/z calcd for C$_{27}$H$_{28}$N$_2$O$_1$ [M−H] $^+$: 396.2196. Found: 396.2193.

Synthesis of Compound 1g. 3-methoxyaniline **3d** (381.2 mg, 3.10 mmol) and compound **2a** (200.5 mg, 0.31 mmol) were placed in a flask containing DMF (3.0 mL). After heating for 4 h at 150 °C under nitrogen, the solution was concentrated under reduced pressure. The resulting crude product was purified by silica gel flash chromatography using petroleum ether/CH$_2$Cl$_2$/MeOH (25:25:1) as eluent to give compound **1g** as a red solid (81.6 mg; yield 48.9%). ^{1}H NMR (400 MHz, CDCl$_3$, TMS) δ 8.44 (d, J = 12.8 Hz, 1H), 7.58 (s, 1H), 7.47−7.49 (d, J = 8.8 Hz, 1H), 7.32 (s, 1H), 7.13−7.17 (m, 2H), 6.99−7.02 (m, 1H), 6.82−6.86 (m, 1H), 6.58−6.60 (d, J = 8.0 Hz, 1H), 5.56−5.59 (d, J = 13.2 Hz, 1H), 3.94 (s, 3H), 3.66−3.72 (m, 2H), 2.85 (t, J = 4.2 Hz, 2H), 2.76 (m, 2H), 1.87−1.92 (m, 2H), 1.77 (s, 6H), 1.24 (t, J = 4.2 Hz, 3H). ^{13}C NMR (100 MHz, CDCl$_3$) 159.65, 157.48 155.47, 144.11, 139.16, 133.32, 129.90, 128.50, 127.51, 127.48, 125.24, 125.08, 121.80, 121.50, 119.29, 117.35, 107.69, 106.81, 105.62, 103.64, 100.76, 92.53, 55.26, 45.76, 36.61, 30.37, 28.60, 26.23, 22.32, 10.86. HRMS (EI) m/z calcd for C$_{28}$H$_{31}$N$_2$O$^+$ [M−H] $^+$: 410.2353. Found: 410.2344.

Synthesis of Compound NIR-H$_2$O$_2$. Compound **1e** (110 mg, 0.226 mmol) and CsCO$_3$ (130 mg, 0.678 mmol) were dissolved in CH$_2$Cl$_2$. The mixture was stirred at room temperature for 10 min, and then compound **9** (180 mg, 0.678 mmol) was added. After overnight reaction, the solvent was removed under reduced pressure. The resulting residue was purified by a silica gel column (CH$_2$Cl$_2$/C$_2$H$_5$OH = 10:1) to afford compound **NIR-H$_2$O$_2$** as a blue solid (102.9 mg, isolated yield: 65.7%): ^{1}H NMR (500 Hz, MeOD): δ = 1.37−1.40 (t, J = 7.5 Hz, 3H), 1.7 (s, 6H), 1.8−1.82 (t, J = 6.0 Hz, 2H), 2.58−2.6 (t, J = 6 Hz, 2H), 2.62 −2.65 (t, J = 6 Hz, 2H), 4.30−4.34 (d, J = 7 Hz, 2H), 5.25 (s, 2H), 6.41−6.44 (d, J = 15 Hz, 1H), 7.0 (s, 1H), 7.11 (s, 1H), 7.37−7.50 (6H), 7.59−7.6 (d, J = 7 Hz, 2H), 7.7−7.72(d, J = 7.5 Hz, 1H), 8.54−8.57 (d, J = 14.0 Hz,1H). ^{13}C NMR (125 Hz, MeOD): 10.22, 13.97, 19.6, 22.52, 26.00, 29.15, 31.14, 42.65, 53.24, 59.33, 71.78, 73.71, 103.89, 106.37, 112.19, 114.98, 116.88, 118.50, 122.60, 124.86, 128.32, 129.78, 130.12, 130.90, 131.34, 133.90, 136.45, 143.43, 144.84, 148.41, 155.06, 159.16, 163.10, 180.33. HRMS (ESI) m/z calcd for C$_{34}$H$_{34}$*B$_1$Cl$_1$N$_1$O$_4$ ([M]): 565.2300. Found: 565.2317.

Synthesis of Compound NIR-thiol. To a solution of compound **1a** (100.0 mg, 0.19 mmol) and 2,4-dinitrobenzenesulfonyl chloride (203.4 mg, 0.76 mmol) in dry CH$_2$Cl$_2$ (10 mL), Cs$_2$CO$_3$ (30.1 mg, 0.091 mmol) was added. The mixture was stirred at room temperature for 30 min, and then the solvent was evaporated under reduced pressure to give the crude product, which was purified on a basic Al$_2$O$_3$ column eluted with CH$_2$Cl$_2$/C$_2$H$_5$OH (100:1 to 30:1) to yield compound **NIR-thiol** as a blue solid (85.9 mg, yield 60.0%). ^{1}H NMR (400 MHz, CDCl$_3$): δ 1.54−1.57 (t, 3H), 1.81 (s, 6H), 1.90 (2H), 2.72 (4H), 4.54−4.56 (q, J = 7.2 Hz, 2H), 6.64−6.68 (d, J = 15.2 Hz, 1H), 7.02−7.04 (2H), 7.21 (s, 1H), 7.37−7.39 (d, J = 8.4 Hz, 1H), 7.46−7.50 (2H), 7.51−7.57 (2H), 8.23 (d, J = 2.0 Hz, 1H), 8.26−8.29 (1H), 8.32−8.35 (d, J = 8.8 Hz, 1H), 8.38−8.40 (d, J = 8.8 Hz, 1H),

8.60−8.66 2H), 8.68 (s, 1H). ^{13}C NMR (125 MHz, CDCl$_3$): δ 13.16, 20.07, 24.11, 27.78, 28.93, 29.48, 41.69, 51.36, 106.68, 110.10, 113.31, 115.72, 118.23, 118.69, 120.52, 121.68, 122.74, 125.29, 127.42, 128.39, 128.81, 128.94, 129.46, 129.66, 130.91, 131.56, 131.86, 133.05, 134.39, 140.79, 142.48, 145.36, 146.60, 147.45, 148.21, 148.83, 149.49, 151.14, 152.92, 158.79, 167.79, 178.65. HRMS (ESI) m/z calcd for $C_{33}H_{30}N_3O_8S^+$ (M$^+$): 628.1748. Found: 628.1749.

Spectroscopic Studies of the Sensor NIR-H$_2$O$_2$. Superoxide (O$_2^{\cdot-}$) was added as solid KO$_2$. Hydroxyl radical and *tert*-butoxy radical ($\cdot$O^{t}Bu) were generated by reaction of Fe^{2+} with H$_2$O$_2$ or TBHP, respectively.[21b] Nitric oxide (NO) was generated from DEA/NONOate (stock solution 1 mM in 0.01 M NaOH).[29] Singlet oxygen (^{1}O$_2$) was generated from ClO$^-$ and H$_2$O$_2$.[30] A stock solution of DEA/NONOate was prepared in 0.01 M NaOH solution. Various analytes represented by H$_2$O$_2$, NO$_3^-$, NO$_2^-$, HClO, O$_2^{\cdot-}$, $\cdot$OH, ^{1}O$_2$, CH$_3$COOOH, NO, Fe^{3+}, GSH, TBHP, vitamin C,$\cdot$O^{t}Bu were added to the solution of **NIR-H$_2$O$_2$** (final concentration, 1 μM) in 0.1 M PBS, pH 7.4 (containing 1% DMSO). The resulting solution was kept at ambient temperature for 30 min, and then the fluorescence intensities were recorded with excitation at 690 nm.

Raw 264.7 Murine Macrophages Culture and Imaging Using NIR-H$_2$O$_2$. Raw 264.7 murine macrophages were obtained from a Xiangya hospital and cultured in Dulbecco's modified eagle medium (DMEM) supplemented with 10% FBS (fetal bovine serum) in an atmosphere of 5% CO$_2$ and 95% air at 37 °C. For detection of endogenously produced H$_2$O$_2$, the living RAW 264.7 macrophages were coincubated with PMA (1 μg/mL), **NIR-H$_2$O$_2$** (1 μM), Hoechst 33258 (4.5 μM), and mito tracker green (1 μM) for 60 min. Prior to imaging, the cells were washed 3× with 1 mL of PBS, and the fluorescence images were acquired through an Olympus fluorescence microscopy equipped with a cooled CCD camera.

Fluorescent Imaging in Living Mice Using NIR-H$_2$O$_2$. ICR mice, 20−25 g, were given an ip injection of LPS (1 mg in 400 μL saline). After 4 h, the mice were anesthetized by an ip injection of xylazine (10 mg/kg) and ketamine (80 mg/kg), and the abdominal fur was removed with an electric shaver. Then, the mice were intraperitoneally injected with **NIR-H$_2$O$_2$** (400 μM in 400 μL of 1:9 = DMSO:PBS). As a control, untreated (neither treated with LPS nor **NIR-H$_2$O$_2$**) or unstimulated mice ip injected only with **NIR-H$_2$O$_2$** (400 μM in 400 μL of 1: 9 = DMSO: PBS) were also prepared. The mice were then imaged (30 min after the injection of **NIR-H$_2$O$_2$**) by using a FMT 2500 LX quantitative tomography *in vivo* imaging system, with an excitation filter of 670 nm and an emission filter of 690−740 nm.

Bel 7702 Cells Incubation and Fluorescence Imaging Using NIR-thiol. Bel 7702 cells were cultured in DMEM supplemented with 10% FBS in an atmosphere of 5% CO$_2$ and 95% air at 37 °C. One day before imaging, the cells were seeded in 24-well flat-bottomed plates in an atmosphere of 5% CO$_2$, 95% air at 37 °C for 24 h. The cells were incubated with the sensor **NIR-thiol** (5 μM) and Hoechst 33258 (4.5 μM) for 30 min at 37 °C in PBS buffer (containing 1% DMSO) and then washed with PBS buffer 3×. For the control experiment, the cells were pretreated with PBS solution containing *N*-ethylmaleimide (1 mM) for 30 min, and then incubated with the sensor **NIR-thiol** (5 μM) in PBS (containing 1% DMSO) for 30 min at 37 °C. Fluorescence imaging was then carried out after washing cells with PBS. Fluorescence imaging of intracelluar thiols was conducted using a Nikon eclipse TE300 inverted fluorescence microscope.

Fluorescent Imaging in Living Mice Using NIR-thiol. ICR mice, 20−25 g, were ip injected with a different amount of **NIR-thiol** (0, 20, 40, or 160 nanomoles) in 100 μL of 1:3 = DMSO:PBS. Subsequently, the mice were anesthetized by ip injection of xylazine (10 mg/kg) and ketamine (80 mg/kg), and their abdominal fur was removed with an electric shaver. The mice were then imaged by using a FMT 2500 LX quantitative tomography *in vivo* imaging system, with an excitation filter of 670 nm and an emission filter of 690−740 nm.

■ ASSOCIATED CONTENT

⑤ Supporting Information

Experimental procedures and some spectra. This material is available free of charge via the Internet at http://pubs.acs.org.

■ AUTHOR INFORMATION

Corresponding Author

weiyinglin@hnu.edu.cn

Notes

The authors declare no competing financial interest.

■ ACKNOWLEDGMENTS

■ REFERENCES

(1) (a) Lichtman, J. W.; Conchello, J. A. *Nat. Methods* **2005**, *2*, 910−919. (b) Ghoroghchian, P. P.; Therien, M. J.; Hammer, D. A. *Nanomed. Nanobiotechnol.* **2009**, *1*, 156−167. (c) Valeur, B. *Molecular Fluorescence: Principles and Applications*; Wiley-VCH: Weinheim, Germany, 2001.

(2) For some reviews, see: (a) Loudet., A.; Burgess, K. *Chem. Rev.* **2007**, *107*, 4891−4932. (b) Goncalves., M. S. T. *Chem. Rev.* **2009**, *109*, 190−212. (c) Qian, X.; Xiao, Y.; Xu, Y.; Guo, X.; Qian, J.; Zhu, W. *Chem. Commun.* **2010**, *46*, 6418−6436.

(3) For some recent examples, see: (a) Qian, Y.; Karpus, J.; Kabil, O.; Zhang, S. Y.; Zhu, H. L.; Banerjee, R.; Zhao, J.; He, C. *Nat. Commun.* **2011**, *2*, 495. (b) Yang, Y.; Lowry, M.; Xu, X.; Escobedo, J. O.; Sibrian-Vazquez, M.; Wong, L.; Schowalter, C. M.; Jensen, T. J.; Fronczek, F. R.; Warner, I. M.; Strongin, R. M. *Proc. Natl. Acad. Sci. U.S.A.* **2008**, *105*, 8829−8834. (c) Palama, I.; DiMaria, F.; Viola, I.; Fabiano, E.; Gigli, G.; Bettini, C.; Barbarella, G. *J. Am. Chem. Soc.* **2011**, *133*, 17777−17785. (d) Liu, C.; Pan, J.; Li, S.; Zhao, Y.; Wu, L. Y.; Berkman, C. E.; Whorton, A. R.; Xian, M. *Angew. Chem., Int. Ed.* **2011**, *50*, 10327−10329. (e) Peng, X.; Yang, Z.; Wang, J.; Fan, J.; He, Y.; Song, F.; Wang, B.; Sun, S.; Qu, J.; Qi, J.; Yan, M. *J. Am. Chem. Soc.* **2011**, *133*, 6626−6635. (f) Sotgiu, G.; Galeotti, M.; Samor, C.; Bongini, A.; Mazzanti, A. *Chem.—Eur. J.* **2011**, *17*, 7947−7952. (g) Kim, E.; Koh, M.; Ryu, J.; Park, S. B. *J. Am. Chem. Soc.* **2008**, *130*, 12206−12207. (h) Peng, T.; Yang, D. *Org. Lett.* **2010**, *12*, 496−499. (i) Leevy, W. M.; Gammon, S. T.; Jiang, H.; Johnson, J. R.; Maxwell, D. J.; Jackson, E. N.; Marquez, M.; Piwnica-Worms, D.; Smith, B. D. *J. Am. Chem. Soc.* **2006**, *128*, 16476−16477. (j) Li, J.; Yao, S. Q. *Org. Lett.* **2009**, *11*, 405−408. (k) Hapuarachchige, S.; Montano, G.; Ramesh, C.; Rodriguez, D.; Henson, L. H.; Williams, C. C.; Kadavakkollu, S.; Johnson, D. L.; Shuster, C. B.; Arterburn, J. B. *J. Am. Chem. Soc.* **2011**, *133*, 6780−6790. (l) Yuan, L.; Lin, W.; Xie, Y.; Chen, B.; Zhu, S. *J. Am. Chem. Soc.* **2012**, *134*, 1305−1315.

(4) Ueno, T.; Nagano, T. *Nat. Meth.* **2011**, *8*, 642−645.

(5) For some reviews, see: (a) de Silva, A. P.; Gunaratne, H. Q. N.; Gunnlaugsson, T.; Huxley, A. J. M.; McCoy, C. P.; Rademacher, J. T.; Rice, T. E. *Chem. Rev.* **1997**, *97*, 1515−1566. (b) Nolan, E. M.; Lippard, S. J. *Chem. Rev.* **2008**, *108*, 3443−3480. (c) Que, E. L.; Domaille, D. W.; Chang, C. J. *Chem. Rev.* **2008**, *108*, 1517−1549. (d) Quang, D. T.; Kim, J. S. *Chem. Rev.* **2010**, *110*, 6280−6301. (e) Thomas, S. W., III; Joly, G. D.; Swager, T. M. *Chem. Rev.* **2007**, *107*, 1339−1386. (f) Han, J.; Burgess, K. *Chem. Rev.* **2010**, *110*, 2709−2728. (g) Kobayashi, H.; Ogawa, M.; Alford, R.; Choyke, P. L.; Urano, Y. *Chem. Rev.* **2010**, *110*, 2620−2640. (h) Chen, X.; Tian, X.; Shin, I.; Yoon, J. *Chem. Soc. Rev.* **2011**, *40*, 4783−4804. (i) Cho, D.-G.; Sessler, J. L. *Chem. Soc. Rev.* **2009**, *38*, 1647−1662. (j) Kim, H. N.; Lee, M. H.; Kim, H. J.; Kim, J. S.; Yoon, J. *Chem. Soc. Rev.* **2008**, *37*, 1465−1472. (k) Beija, M.; Afonso, C. A. M.; Martinho, J. M. G. *Chem. Soc. Rev.*

2009, 38, 2410–2433. (l) Chen, X.; Pradhan, T.; Wang, F.; Kim, J. S.; Yoon, J. *Chem. Rev.* **2012**, *112*, 1910–1956.

(6) For some books, see: (a) Demchenko, A. P. *Introduction to Fluorescence Sensing*; Springer: New York, 2008. (b) Wang, B.; Anslyn., E. V. *Chemosensors: Principles, Strategies, and Applications*; Wiley: Hoboken, NJ, 2011.

(7) For some books and reviews, see: (a) *Near-Infrared Applications in Biotechnology*; Raghavachari, R., Ed.; Marcel Dekker: New York, 2001. (b) Weissleder, R. *Nat. Biotechnol.* **2001**, *19*, 316–317. (c) Frangioni., J. V. *Curr. Opin. Chem. Biol.* **2003**, *7*, 626–634. (g) Escobedo, J. O.; Rusin, O.; Lim, S.; Strongin, R. M. *Curr. Opin. Chem. Biol.* **2010**, *14*, 64–70. (h) Hilderbrand, S. A.; Weissleder, R. *Curr. Opin. Chem. Biol.* **2010**, *14*, 71–79.

(8) For some examples, see: (a) Fischer, G. M.; Daltrozzo, E.; Zumbusch, A. *Angew. Chem., Int. Ed.* **2011**, *50*, 1406–1409. (b) Fischer, G. M.; Ehlers, A. P.; Zumbusch, A.; Daltrozzo, E. *Angew. Chem., Int. Ed.* **2007**, *46*, 3750–3753. (c) Qin, W.; Ding, D.; Liu, J.; Yuan, W. Z.; Hu, Y.; Liu, B.; Tan, B. Z. *Adv. Funct. Mater.* **2012**, *22*, 771–779. (d) Umezawa, K.; Nakamura, Y.; Makino, H.; Citterio, D.; Suzuki, K. *J. Am. Chem. Soc.* **2008**, *130*, 1550–1551. (e) Baumes, J. M.; Gassensmith, J. J.; Giblin, J.; Lee, J.-J.; White, A. G.; Culligan, W. J.; Leevy, W. M.; Kuno, M.; Smith, B. D. *Nat. Chem* **2010**, *2*, 1025–1030. (f) Bürckstümmer, H.; Kronenberg, N. M.; Meerholz, K.; Würthner, F. *Org. Lett.* **2010**, *12*, 3666–3669. (g) Bouit, P.; Piazza, E. D.; Rigaut, S.; Guennic, B. L.; Aronica, C.; Toupet, L.; Andraud, C.; Maury, O. *Org. Lett.* **2008**, *10*, 4159–4162. (h) Toutchkine, A.; Nguyen, D.-V.; Hahn, K. M. *Bioconjugate Chem.* **2007**, *18*, 1344–1348. (i) McDonnell, S. O.; O'Shea, D. F. *Org. Lett.* **2006**, *8*, 3493–3496. (j) Kundu, K.; Knight, S. F.; Willett, N.; Lee, S.; Taylor, W. R.; Murthy, N. *Angew. Chem., Int. Ed.* **2009**, *48*, 299–303. (k) Descalzo, A. B.; Xu, H.-J.; Xue, Z.-L.; Hoffmann, K.; Shen, Z.; Weller, M. G.; You, X.-Z.; Rurack, K. *Org. Lett.* **2008**, *10*, 1581–1584. (l) Bai, M.; Achilefu, S. *Bioorg. Med. Chem. Lett.* **2011**, *21*, 280–284. (m) Zhang, Z.; Berezin, M. Y.; Kao, J. L. F.; d'Avignon, A.; Bai, M.; Achilefu, S. A. *Angew. Chem., Int. Ed.* **2008**, *47*, 3584–3587. (n) Yuan, L.; Lin, W.; Yang, Y.; Chen, H. *J. Am. Chem. Soc.* **2012**, *134*, 1200–1211. (o) Olivier, J.-H.; Widmaier, J.; Ziessel, R. *Chem.—Eur. J.* **2011**, *17*, 11709–11714.

(9) For some examples, see: (a) Sasaki, E.; Kojima, H.; Nishimatsu, H.; Urano, Y.; Kikuchi, K.; Hirata, Y.; Nagano, T. *J. Am. Chem. Soc.* **2005**, *127*, 3684–3685. (b) Kiyose, K.; Aizawa, S.; Sasaki, E.; Kojima, H.; Hanaoka, K.; Terai, T.; Urano, Y.; Nagano, T. *Chem.—Eur. J.* **2009**, *15*, 9191–9200.

(10) For some reviews and examples, see: (a) Reymond, J. L.; Fluxà, V. S.; Maillard, N. *Chem. Commun.* **2009**, 34–46. (b) Song, F.; Garner, A. L.; Koide, K. *J. Am. Chem. Soc.* **2007**, *129*, 12354–12355. (c) Kamiya, M.; Kobayashi, H.; Hama, Y.; Koyama, Y.; Bernardo, M.; Nagano, T.; Choyke, P. L.; Urano, Y. *J. Am. Chem. Soc.* **2007**, *129*, 3918–3929. (d) Lavis, L, D.; Raines, R. T. *ACS Chem. Biol.* **2008**, *3*, 142–155. (e) Huang, S.-T.; Teng, C.-J.; Lee, Y.-H.; Wu, J.-Y.; Wang, K.-L.; Lin, C.-M. *Anal. Chem.* **2010**, *82*, 7329–7334. (f) Lavis, L. D.; Chao, T.-Y.; Raines, R. T. *Chem. Sci.* **2011**, *2*, 521–530. (g) Taki, M.; Iyoshi, S.; Ojida, A.; Hamachi, I.; Yamamoto, Y. *J. Am. Chem. Soc.* **2010**, *132*, 5938–5939. (h) Chen, X.; Sun, M.; Ma, H. *Curr. Org. Chem.* **2006**, *10*, 477–489. (i) Razgulin, A.; Ma, N.; Rao, J. *Chem. Soc. Rev.* **2011**, *40*, 4186–4216.

(11) Wolinska, E.; Henary, M.; Paliakov, E.; Strekowski, L. *J. Heterocycl. Chem.* **2009**, *46*, 925–930.

(12) The pK_a was calculated according to the Henderson–Hasselbach-type mass action equation ($\log[(F_{max} - F)/(F - F_{min})]$ = pK_a – pH).

(13) (a) Bouit, P.-A.; Aronica, C.; Toupet, L.; Guennic, B. L.; Andraud, C.; Maury, O. *J. Am. Chem. Soc.* **2010**, *132*, 4328–4335. (b) Würthner, F.; Archetti, G.; Schmidt, R.; Kuball, H.-G. *Angew. Chem., Int. Ed.* **2008**, *47*, 4529–4532.

(14) (a) Valeur, B. *Molecular Fluorescence: Principles and Applications*, Wiley-VCH: Weinheim, Germany, 2001. (b) Magde, D.; Rojas, G. E.; Seybold, P. *Photochem. Photobiol.* **1999**, *70*, 737–744. (c) Oushiki, D.; Kojima, H.; Terai, T.; Arita, M.; Hanaoka, K.; Urano, Y.; Nagano, T. *J. Am. Chem. Soc.* **2010**, *132*, 2795–2801.

(15) (a) Champagne, B.; Guillaume, M.; Zutterman, F. *Chem. Phys. Lett.* **2006**, *425*, 105–109. (b) Benzi, C.; Bertolino, C. A.; Miletto, I.; Ponzio, P.; Barolo, C.; Viscardi, G.; Coluccia, S.; Caput, G. *Dyes and Pigments* **2009**, *83*, 111–120.

(16) (a) Bashan, N.; Kovsan, J.; Kachko, I.; Ovadia., H.; Rudich, A. *Physiol. Rev.* **2009**, *89*, 27–71. (b) Kuznetsov, A. V.; Kehrer, I.; Kozlov, A. V.; Haller, M.; Redl, H.; Hermann, M.; Grimm, M.; Troppmair, J. *Anal. Bioanal. Chem.* **2011**, *400*, 2383–2390. (c) Pandey, A. N.; Tripathi, A.; PremKumar, K. V.; Shrivastav, T. G.; Chaube, S. K. *J. Cell. Biochem.* **2010**, *111*, 521–528. (d) Peyrot, F.; Ducrocq, C. *J. Pineal Res.* **2008**, *45*, 235–246. (e) Rhee, S. G. *Science.* **2006**, *312*, 1882–1883. (f) Reth, M. *Nat. Immun.* **2002**, *3*, 1129–1134. (g) Rhee, S. G. *Exp. Mol. Med.* **1999**, *31*, 53–59. (h) Stone, J. R.; Yang, S. *Antioxid. Redox Signaling* **2006**, *8*, 243–270.

(17) (a) Winterbourn, C. C. *Nat. Chem. Biol.* **2008**, *4*, 278–286. (b) Paulsen, C. E.; Carroll, K. S. *ACS Chem. Biol* **2010**, *5*, 47–62. (c) Miller, E. W.; Dickinson, B. C.; Chang, C. J. *Proc. Natl. Acad. Sci. U.S.A.* **2010**, *107* (36), 15681–15686. (d) D'Autréaux, B.; Toledano, M. B.. *Nat. Rev. Mol. Cell. Biol.* **2007**, *8*, 813–824.

(18) Galaris, D.; Skiada, V.; Barbouti, A. *Cancer Lett.* **2008**, *266*, 21–29.

(19) Lin, M. T.; Beal, M. F. *Nature* **2006**, *443*, 787–795.

(20) For some reviews, see: (a) Miller, E. W.; Chang, C. J. *Curr. Opin. Chem. Biol.* **2007**, *11*, 620–625. (b) Chen, X.; Tian, X.; Shin, I.; Yoon, J. *Chem. Soc. Rev.* **2011**, *40*, 4783–4804. (c) McQuade, L. E.; Lippard, S. J. *Curr. Opin. Chem. Biol.* **2010**, *14*, 43–49. (d) Lippert, A. R.; Van De Bittner, G. C.; Chang, C. J. *Acc. Chem. Res.* **2011**, *44*, 793–804.

(21) For some recent examples, see: (a) Dickinson, B. C.; Huynh, C.; Chang, C. J. *J. Am. Chem. Soc.* **2010**, *132*, 5906–5915. (b) Srikun, D.; Miller, E. W.; Domaille, D. W.; Chang, C. J. *J. Am. Chem. Soc.* **2008**, *130*, 4596–4597. (c) Abo, M.; Urano, Y.; Hanaoka, K.; Terai, T.; Komatsu, T.; Nagano, T. *J. Am. Chem. Soc.* **2011**, *133*, 10629–10637. (d) Du, L.; Ni, N.; Li, M.; Wang, B. *Tetrahedron Lett.* **2010**, *51*, 1152–1154. (e) Xu, K. H.; Liu, F.; Wang, H. X.; Wang, S. S.; Wang, L. L.; Tang, B. *Sci China Ser B-Chem* **2009**, *52*, 734–740. (f) Karton-Lifshin, N.; Segal, E.; Omer, L.; Portnoy, M.; Satchi-Fainaro, R.; Shabat, D. *J. Am. Chem. Soc.* **2011**, *133*, 10960–10965. (g) Chung, C.; Srikun, D.; Lim, C. S.; Chang, C. J.; Cho, B. R. *Chem. Commun* **2011**, *47*, 9618–9620.

(22) Li, H.; Li, Q.; Wang, X.; Xu, K.; Chen, Z.; Gong, X.; Liu, X.; Tong, L.; Tang, B. *Anal. Chem.* **2009**, *81*, 2193–2198.

(23) Lee, D.; Khaja, S.; Velasquez-Castano, J. C.; Dasari, M.; Sun, C.; Petros, J.; Taylor, W. R.; Murthy, N. *Nat. Mater.* **2007**, *6*, 765–769.

(24) Beiser, A.; Selhub, J.; Jacques, P. F.; Rosenberg, I. H.; D'Agostino, R. B.; Wilson, P. W. F..; Wolf, P. A. *N. Engl. J. Med.* **2002**, *346*, 476–483.

(25) Ball, R. O.; Courtney-Martin, G.; Pencharz, P. B. *J. Nutr.* **2006**, *136*, 1682S–1693S.

(26) For a review and some examples, see: (a) Chen, X.; Zhou, Y.; Peng, X.; Yoon, J. *Chem. Soc. Rev.* **2010**, *39*, 2120–2135. (b) Sreejith, S.; Divya, K. P.; Ajayaghosh, A. *Angew. Chem., Int. Ed.* **2008**, *47*, 7883. (c) Zhang, M.; Yu, M.; Li, F.; Zhu, M.; Li, M.; Gao, Y.; Li, L.; Liu, Z.; Zhang, J.; Zhang, D.; Yi, T.; Huang, C. *J. Am. Chem. Soc.* **2007**, *129*, 10322. (d) Jung, H. S.; Han, J. H.; Pradhan, T.; Kim, S.; Lee, S. W.; Sessler, J. L.; Kim, T. W.; Kang, C.; Kim, J. S. *Biomaterials* **2012**, *33*, 945. (e) Chen, Y.; Zhao, J.; Guo, H.; Xie, L. *J. Org. Chem.* **2012**, *77*, 2192–2206.

(27) Maeda, H.; Matsuno, H.; Ushida, M.; Katayama, K.; Saeki, K *Angew. Chem., Int. Ed.* **2005**, *44*, 2922–2925.

(28) Mosmann, T. *J. Immunol. Meth.* **1983**, *65*, 55–63.

(29) Zhang, X.; Kim, W.-S.; Hatcher, N.; Potgieter, K.; Moroz, L. L.; Gillette, R.; Sweedler, J. V. *J. Biol. Chem.* **2002**, *277*, 48472–48478.

(30) Tang, B.; Zhang, N.; Chen, Z.; Xu, K.; Zhuo, L.; An, L.; Yang, G. *Chem.—Eur. J.* **2008**, *14*, 522–528.